

Tectonics

RESEARCH ARTICLE

10.1029/2020TC006065

Key Points:

- The central East Kunlun Shan is an ideal setting to investigate the tectonic evolution of northern Tibet and plateau-wide geodynamic drivers
- The central East Kunlun Shan experienced crustal shortening from Paleocene–Oligocene time followed by a 23–20 Ma onset of strike-slip faulting
- The plateau-wide mid-Miocene onset of strike-slip and normal faulting signals the attainment of high GPE and elevation

Supporting Information:

- Supporting Information S1

Correspondence to:

L. M. Staisch,
lstaisch@usgs.gov

Citation:

Staisch, L. M., Niemi, N. A., Clark, M. K., & Chang, H. (2020). The Cenozoic evolution of crustal shortening and left-lateral shear in the central East Kunlun Shan: Implications for the uplift history of the Tibetan Plateau. *Tectonics*, 39, e2020TC006065. <https://doi.org/10.1029/2020TC006065>

Received 13 JAN 2020

Accepted 29 JUN 2020

Accepted article online 1 JUL 2020

The Cenozoic Evolution of Crustal Shortening and Left-Lateral Shear in the Central East Kunlun Shan: Implications for the Uplift History of the Tibetan Plateau

Lydia M. Staisch^{1,2} , Nathan A. Niemi¹ , Marin K. Clark¹, and Hong Chang³ 

¹Department of Earth and Environmental Sciences, University of Michigan, Ann Arbor, MI, USA, ²Now at Geology Minerals Energy and Geophysics Science Center, U.S. Geological Survey, Portland, OR, USA, ³Institute of Earth Environment, CAS, Xi'an, China

Abstract The timing of crustal shortening and strike-slip faulting along the East Kunlun Shan provides insight into the history of surface uplift and may constrain the time at which the Tibetan Plateau reached high elevations. We investigate a series of extensional basins and restraining bends along the Xidatan strand of the Kunlun strike-slip fault, which provide an ideal setting to unravel the tectonic history of the northern plateau margin. We present new apatite (U-Th)/He, apatite fission track, and zircon (U-Th)/He ages and QTQt thermal modeling, ⁴⁰Ar/³⁹Ar fault gouge dating, and structural mapping from the central East Kunlun Shan. Our data suggest that the East Kunlun Shan experienced slow to negligible exhumation until late Cretaceous time, followed by an increase in rate by 65–50 Ma. Along with a ~47 Ma fault gouge age, we posit that the Paleocene–early Eocene was a time of crustal shortening along the northern plateau. Rapid exhumation along transpressional portions of the Xidatan fault initiated by 23–20 Ma, which we interpret as the local onset of strike-slip faulting. An early Miocene transition from north-south crustal shortening to left-lateral shear along the East Kunlun Shan, the onset of normal and strike-slip faulting in central and southern Tibet by 18 Ma, and lower crustal flow in eastern Tibet by 13 Ma suggest the establishment of orogen-wide east-west oriented extension and extrusion by the middle Miocene. The plateau-wide shift in stress accommodation implies that high gravitational potential energy, and likely high elevation, was attained by the middle Miocene.

1. Introduction

The timing of onset of strike-slip faulting within the East Kunlun Shan, located along the northern margin of the Tibetan Plateau, is an outstanding controversy with significant implications for unraveling the tectonic evolution of the Himalayan-Tibetan orogen. Currently, the Kunlun fault accommodates convergence between India and Eurasia via left-lateral shear at a rate of ~10–11 mm yr⁻¹ (Avouac & Tapponnier, 1993; Kirby et al., 2007; Li et al., 2005; van der Woerd et al., 1998, 2000, 2002). However, the East Kunlun Shan was previously the site of north-south oriented pure shear deformation, which is suggested to have initiated between 41 and 27 Ma (Clark et al., 2010; Duvall et al., 2011; Jolivet et al., 2003; Mock et al., 1999; Shi et al., 2018; Wang et al., 2004, 2017; Wu et al., 2009; Yin et al., 2007). The transition in structural style, from crustal thickening to eastward extrusion, along the East Kunlun Shan indicates a shift in the orientation of principal stresses. This kinematic change may directly relate to the attainment of high elevation and associated high gravitational potential energy of the northern Tibetan Plateau (Burke & Sengor, 1986; Platt & England, 1994; Rey et al., 2001). Few constraints exist on the timing of the switch from predominantly pure shear to simple shear deformation or when northern Tibet attained high elevation, thus fueling debate about when and how the Tibetan Plateau was uplifted to its modern elevation.

While most studies agree that left-lateral shear in the East Kunlun Shan initiated in the Cenozoic, there is uncertainty about the exact timing of onset (Dai et al., 2013; Duvall et al., 2013; Fu & Awata, 2007; Jolivet et al., 2003; Kidd & Molnar, 1988; Wu et al., 2001). Several studies infer that strike-slip faulting initiated in Plio-Pleistocene time based on the offset of fluvial and glacial features (Kidd & Molnar, 1988; Wu et al., 2001), while others infer ~10 Ma initiation of shear based on fault displacement and extrapolation of the modern fault slip rate (Fu & Awata, 2007). Uncertainties in both the timing of geomorphic feature

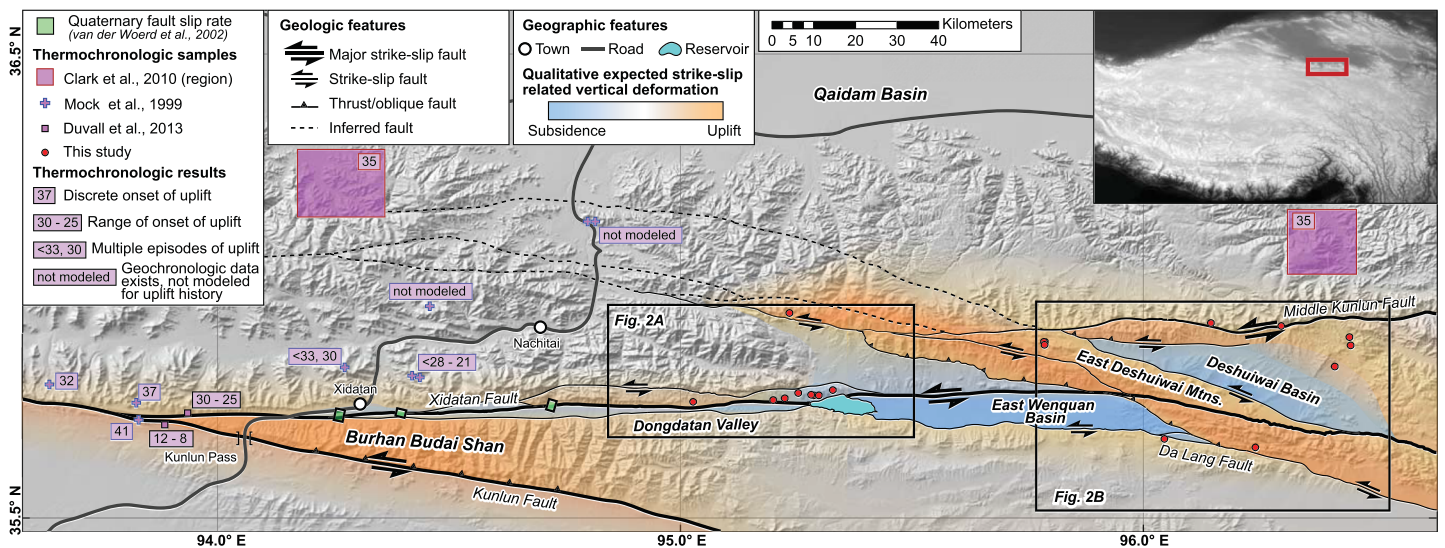


Figure 1. Hillshade map of the central East Kunlun Shan with the general location marked in the inset map of the Tibetan Plateau. Active strike-slip faults and oblique-slip faults are shown. Thermochronologic and fault slip rate studies are denoted for reference. The modeled timing of initial rapid cooling, in millions of years, for samples from Mock et al. (1999), Clark et al. (2010), and Duvall et al. (2013) are outlined in blue, red, and black, respectively. Single numbers represent a well-constrained modeled onset of uplift, whereas numbers separated by a hyphen represent a period of time during which the onset of uplift is modeled to have occurred. Numbers separated by a comma represent potential multiple stages of uplift. Locations labeled “not modeled” indicate sample locations for which geochronologic data exist but was not modeled for uplift history. Thermochronologic samples from this study are marked in red. The orange-blue gradient overlay qualitatively shows expected vertical uplift and subsidence related to recent strike-slip fault motion. The assignment of strike slip-related vertical motion was assessed by comparing regional topographic patterns, known strike-slip fault locations from prior geologic mapping (Qinghai Bureau of Geology and Mineral Resources [QBGM], 1980, 1981; van der Woerd et al., 2002), and observations of strike slip-related vertical motion in field and theoretical studies (Biddle & Christie-Blick, 1985; Bilham & King, 1989; Chinnery, 1965; Crowell, 1974). The locations of geologic maps in Figure 2 are indicated.

development and in potential variations of the long-term slip history of the Kunlun fault result in uncertainties in estimates of the onset of shear. Alternatively, the timing of magmatism associated with extensional features near the Kunlun fault has been used to infer shear onset at 15 Ma (Jolivet et al., 2003). These volcanic constraints provide a minimum age for the onset of shear and suggest an older onset of faulting than interpretations from offset features and fault displacement (Fu & Awata, 2007; Kidd & Molnar, 1988; Wu et al., 2001). The initiation of shear at 20–15 Ma, with a possible phase from 30–20 Ma, is inferred from the initiation of rapid cooling from thermochronologic data (Dai et al., 2013; Duvall et al., 2013). However, difficulty in isolating the onset of strike-slip motion from the earlier, multiphase deformation history of the northern plateau margin may lead to overestimates in the timing of strike-slip fault onset, particularly when using exhumation of discrete fault blocks as a proxy for the onset of lateral shear. An additional complicating factor is the heterogeneous onset of strike-slip faulting along the >1,000 km length of the Kunlun fault, as inferred by Duvall et al. (2013). To unravel the kinematic history of the East Kunlun Shan, detailed structural analyses of faulting style in concert with age constraints on exhumation from thrust and strike-slip motion are necessary.

In this study, we present new low-temperature thermochronologic data and modeling from the central Kunlun fault zone and $^{40}\text{Ar}/^{39}\text{Ar}$ fault gouge dating to assess the tectonic evolution of the northern margin of the Tibetan Plateau. Strike-slip motion within the East Kunlun Shan has produced localized basin subsidence in en echelon rhombochasms and uplift along restraining bends, steps, and fault junctions (Figure 1; Duvall et al., 2013; Fu & Awata, 2007), such as along the Xidatan segment of the Kunlun fault between the Dongdatan Valley and Deshuwai Basin (Figure 1). We focus our work along this section of the Kunlun fault because thrust faults are well exposed throughout the region and are commonly crosscut by major and subordinate strike-slip faults, and exposures found in extensional step overs are ideal for isolating the timing of crustal shortening in the East Kunlun Shan. Additionally, restraining bends and fault junctures may concentrate strike slip-related vertical exhumation and are ideal for constraining the initiation of strike-slip faulting. Along with structural mapping and previous work on normal and strike-slip fault initiation, these data clarify the timing of stress reorganization throughout the Tibetan Plateau and provide the opportunity to link this shift to the attainment of high gravitational potential energy via surface uplift.

2. Geologic Setting

The East Kunlun Shan forms a boundary between the high-elevation (>4.5 km), low-relief surfaces of the Tibetan Plateau to the south and the moderate elevation Qaidam Basin (~2.5 km) to the north (Figure 1). Originating as a Paleozoic suture between the Kunlun-Qaidam and Songpan-Ganzi terranes, the East Kunlun Shan is a long-lived tectonic boundary that has experienced multiple periods of tectonic reactivation, including Cretaceous shearing (Chen et al., 2002; Mock et al., 1999), Eocene–Oligocene crustal shortening (Clark et al., 2010; Wu et al., 2009; Yin et al., 2008), and recent left-lateral shear (van der Woerd et al., 1998, 2002). The multistage tectonic history of the East Kunlun Shan has resulted in a complex structural evolution with a diverse assemblage of rock types. Perhaps the most complete record of this complex history is found within the central portion of the East Kunlun Shan, where the Kunlun fault and subordinate fault splays have produced a series of structurally controlled basins and narrow, intervening ranges.

2.1. Geologic Units

We focused our geologic mapping, structural analysis, and sample collection in the central East Kunlun Shan from the Dongdatan Valley in the west to the Deshuiwai Basin in the east. Rock units range from Proterozoic to Quaternary in age (Figures 1 and 2; Qinghai Bureau of Geology and Mineral Resources [QBGMR], 1980, 1981). Below we describe sedimentary and metasedimentary units followed by igneous units exposed in the study area, organized from oldest to youngest.

2.1.1. Sedimentary and Metasedimentary Units

The Proterozoic Wanbaoguo Group, which largely consists of limestone, dolomite, and shale, is crosscut by mafic dikes and is exposed north of the Middle Kunlun fault (Figures 1 and 2b; Qinghai Bureau of Geology and Mineral Resources [QBGMR], 1980, 1981). The Carboniferous Haoteluowa Group is composed largely of marine carbonate with interbedded sandstone and shale and unconformably overlies the Wanbaoguo Group (Qinghai Bureau of Geology and Mineral Resources [QBGMR], 1980, 1981). Within our field area, the Haoteluowa Group is exposed in fault contact with both Mesozoic and Cenozoic strata (Figures 2a and 3; Qinghai Bureau of Geology and Mineral Resources [QBGMR], 1980, 1981). The Permian Ganjia and Maerzheng groups consist of marine carbonate, often fossiliferous and locally metamorphosed to marble (Qinghai Bureau of Geology and Mineral Resources [QBGMR], 1980, 1981). These units are spatially extensive and form the steep topography to the north of the Dongdatan Valley and in the southeastern East Deshuiwai Mountains (Figure 2). In the following sections, we refer to the Ganjia and Maerzheng units together as Permian carbonates.

The Triassic Babaoshan and Naocangjiangou groups are largely composed of shale, siltstone, and fine to coarse sandstone with limited conglomerate, arkose, fossil-bearing coal layers and interbedded volcanic flows (Qinghai Bureau of Geology and Mineral Resources [QBGMR], 1980, 1981). In many regions, these units have been metamorphosed to greenschist facies (Wu et al., 2009). Regional stratigraphic work suggests that the Babaoshan Group unconformably overlies the Naocangjiangou Group (Wang et al., 2009). A 244 Ma volcanic tephra interbedded within the Naocangjiangou Group provides an early Middle Triassic age for the unit (Wu et al., 2010). We refer to these units together as Triassic metapelites in the following sections. In the east, the Jurassic–Cretaceous Yangqu Group is conformably deposited over the Babaoshan Group, and both units are flat-lying to mildly tilted (Figures 4a and 4b; Qinghai Bureau of Geology and Mineral Resources [QBGMR], 1980, 1981; Wang et al., 2009). Together, the Babaoshan, Naocangjiangou, and Yangqu Groups are part of the A'nyemaqen mélange belt, deposited between the Qaidam block and South Kunlun terrane during the Mesozoic (Wang et al., 2009). The Yangqu Group consists of siltstone, arkosic sandstone, and conglomerate and tends to be brick red with gray-green mottling (Figures 4b and 4c).

Previously, recognition of the Yangqu Group was limited to localities within the East Deshuiwai Mountains. However, our mapping and new age dating suggest that this unit is also exposed in the East Wenquan Basin and in Dongdatan Valley (Figures 2b and 3) where it was previously mapped as Cenozoic terrestrial red bed strata (Qinghai Bureau of Geology and Mineral Resources [QBGMR], 1980, 1981). The Cenozoic age for well-indurated and strongly weathered red bed strata exposed in the Dongdatan Valley and on the north side of Wenquan Hu is called into question by recent detrital zircon analyses, which show zircon populations no younger than 174 Ma with well-defined age peaks at ~250 and ~425 Ma (Wu, Zuza, Chen, et al., 2019). As we will show below, our zircon (U–Th)/He ages in combination with the recent detrital zircon ages support an interpretation for an older depositional age. The new age and unit assignment for these terrestrial red bed strata are reflected in Figures 2a and 3.

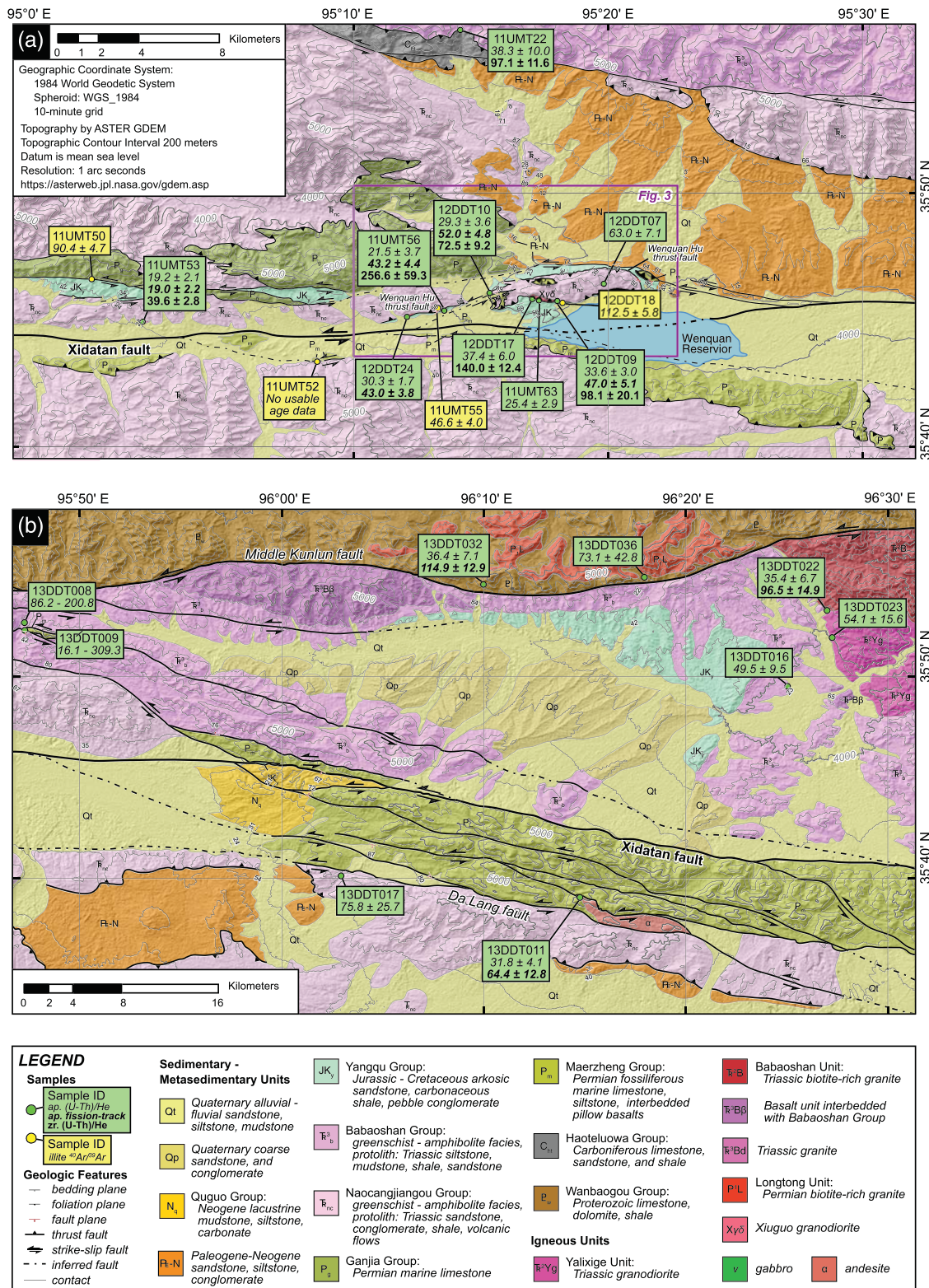


Figure 2. Geologic maps of (a) the Dongdatan Valley and East Wenquan Basin and (b) the East Deshuiwai Mountains and Deshuiwai Basin based on original mapping, published geologic maps (Qinghai Bureau of Geology and Mineral Resources [QBGMR], 1980, 1981), and satellite imagery. Hillshade is based on data from the Advanced Spaceborne Thermal Emission and Reflection Radiometer (ASTER). Fault gouge and thermochronologic samples are shown as yellow and green circles, respectively. Apatite (U-Th)/He ages are printed in italics, apatite fission track ages are printed in bold italics, and zircon (U-Th)/He ages are printed in bold. Most ages reported are mean and standard deviation, except for 13DDT008 and 13DDT009 which are reported as a range due to broad scatter in apatite (U-Th)/He data.

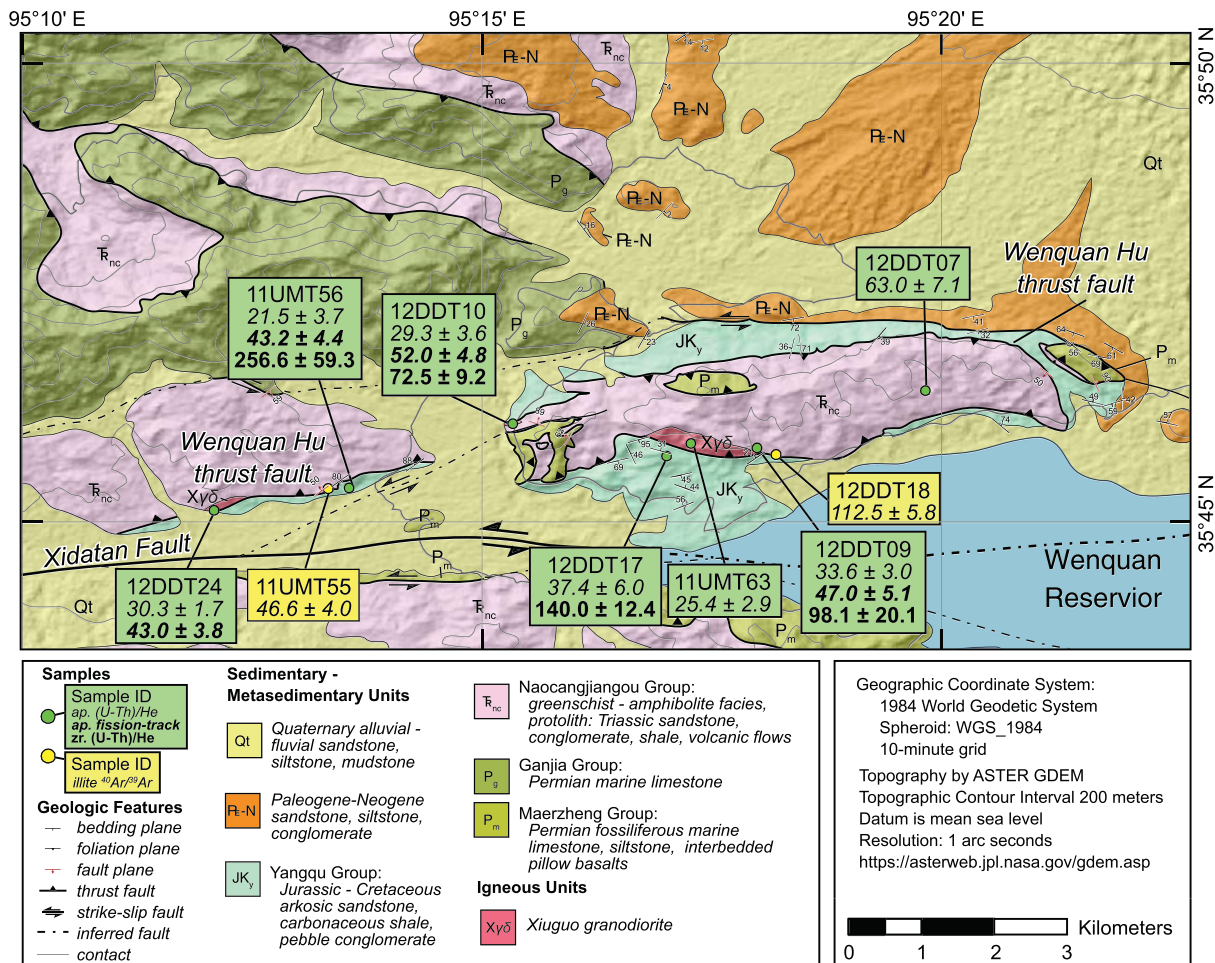


Figure 3. Geologic map of the Dongdatan Valley and East Wenquan Basin based on original mapping, published geologic maps (Qinghai Bureau of Geology and Mineral Resources [QBGMR], 1980, 1981), and satellite imagery. Hillshade and topographic contours are based on ASTER imagery. Fault gouge and thermochronologic samples are shown as yellow and green circles, respectively. Apatite (U-Th)/He ages are printed in italics, apatite fission track ages are printed in bold italics, and zircon (U-Th)/He ages are printed in bold.

Cenozoic strata are unconformably deposited across both Mesozoic and Paleozoic units and are exposed throughout the Dongdatan Valley and East Wenquan Basin, as well as to the south of the East Deshuiwai Mountains (Figures 2, 3, and 4f; Qinghai Bureau of Geology and Mineral Resources [QBGMR], 1980, 1981). The depositional age of Cenozoic strata are not well constrained with absolute age dating. The unnamed Paleogene–Neogene red bed unit is composed of fluvial sandstone, lacustrine siltstone, and conglomerate (Figure 4d) and can be distinguished from the Yangqu Group by its lack of induration, lack of weathering, and absence of green mottling. The Neogene Quguo Group is composed of lacustrine carbonates and fine-grained siltstone and is exposed in the eastern East Wenquan Basin (Qinghai Bureau of Geology and Mineral Resources [QBGMR], 1980, 1981). This unit is characteristically light grayish-yellow to pistachio green in color (Figure 4e).

2.1.2. Igneous Units

Igneous units are exposed throughout the central East Kunlun Shan and range from outcrop-sized plutonic bodies and volcanic flows to large intrusive and extrusive complexes. In the eastern portion of the field area (Figure 2b), Permian granite intrudes the Paleozoic Wanbaoguo Group and is exposed in the high peaks to the north of the Middle Kunlun fault (Qinghai Bureau of Geology and Mineral Resources [QBGMR], 1980, 1981). The Triassic Babaoshan and Yalixige units are granitic and granodioritic intrusive complexes, respectively, over which the Babaoshan Group strata are unconformably deposited (Figure 4a; Qinghai Bureau of Geology and Mineral Resources [QBGMR], 1980, 1981). The Babaoshan Group is interbedded with a thick sequence of basalt flows (Figure 2b), which in some regions exhibits columnar jointing. These basalts are

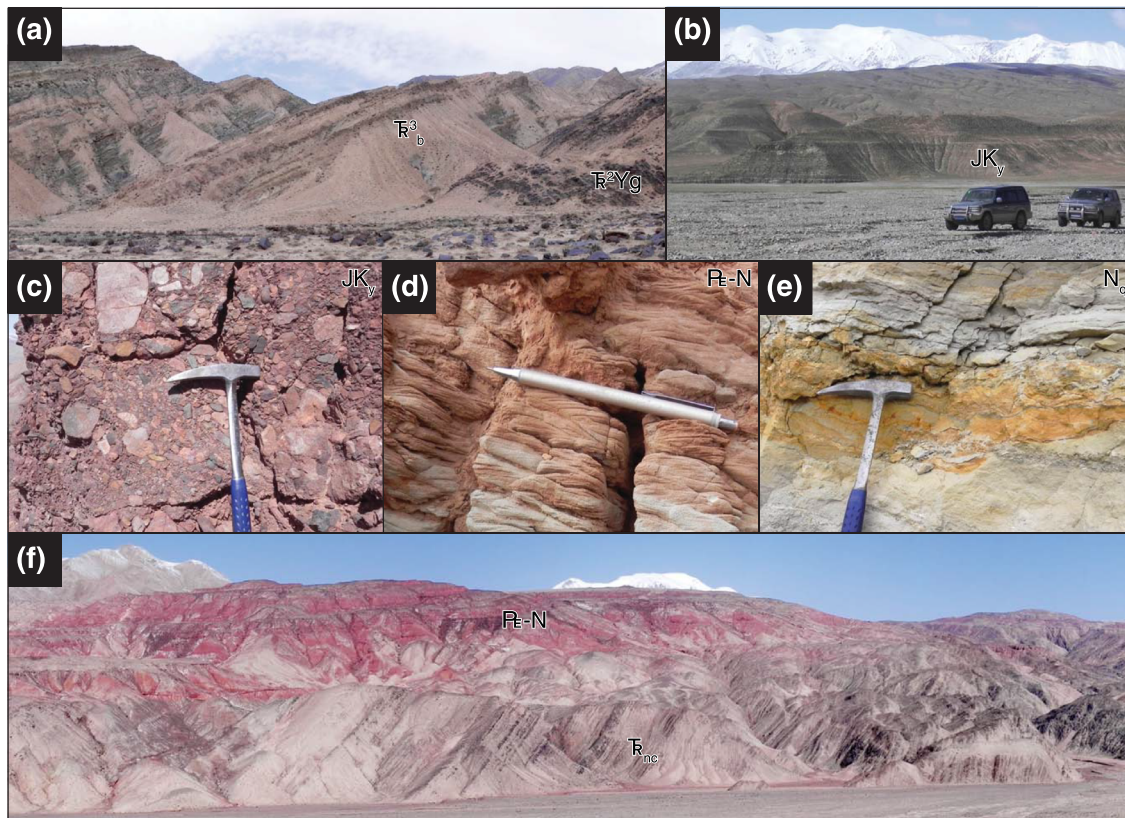


Figure 4. Field photographs of sedimentary features. (a) Tilted Triassic Babaoshan Group unconformably deposited on lower- to mid-Triassic plutonic rocks within the Deshuiwai Basin. (b) Flat-lying Jurassic–Cretaceous Yangqu Group in the central Deshuiwai Basin with sport utility vehicles for scale. (c) Conglomerate of the Yangqu Group showing a heterogeneous source, generally dominated by Permian carbonate and Triassic metapelites. (d) Fine sandstone of the Cenozoic red beds show well-developed cross bedding, indicative of a medium-energy fluvial environment. (e) Finely laminated lacustrine carbonate and carbonate-rich siltstone sequence of the Neogene Quoguo Group. (f) Flat-lying Cenozoic red bed strata are unconformably deposited over steeply dipping and tightly folded Triassic metapelites.

exposed directly south of the Middle Kunlun fault and in the eastern Deshuiwai Basin (Qinghai Bureau of Geology and Mineral Resources [QBGMR], 1980, 1981). Within the western portion of our field area (Figures 2a and 3), igneous units are sparse, small in volume, and generally intrude into the Triassic Naocangjiangou Group (Qinghai Bureau of Geology and Mineral Resources [QBGMR], 1980, 1981). The small intrusions are generally rhyolitic to dacitic in composition and have been moderately metamorphosed along with the host rock. These magmatic intrusions are thought to be associated with Triassic metamorphic overprint in the Xidatan area, dated between 212 and 242 Ma (Liu et al., 2005). Andesitic-dacitic tephra layers are interbedded within the Triassic Naocangjiangou Group and have been dated with U-Pb methods at ~244 Ma (Qinghai Bureau of Geology and Mineral Resources [QBGMR], 1980, 1981; Wu et al., 2010). Where observed in the eastern portion of the field area (Figure 2b), these units tend to be <1 m in thickness. In the southern East Deshuiwai Mountains, a package of andesitic lavas is faulted into place (Figure 2b; Qinghai Bureau of Geology and Mineral Resources [QBGMR], 1980, 1981). The structural complexity associated with the exposure of these andesitic rocks obscures the relationship with any specific sedimentary unit. South of the East Deshuiwai Mountains, small-volume andesitic intrusions are exposed within the Triassic Naocangjiangou Group (Qinghai Bureau of Geology and Mineral Resources [QBGMR], 1980, 1981).

2.2. Structural Geology

2.2.1. North-South Oriented Crustal Shortening

The dominant style of modern deformation in the central East Kunlun Shan is left-lateral strike-slip faulting (Kidd & Molnar, 1988; Molnar & Tapponnier, 1978); however, evidence for north-south contraction is also preserved (Wu et al., 2007, 2009). Throughout the study region, the Carboniferous Haoteluowa Group and

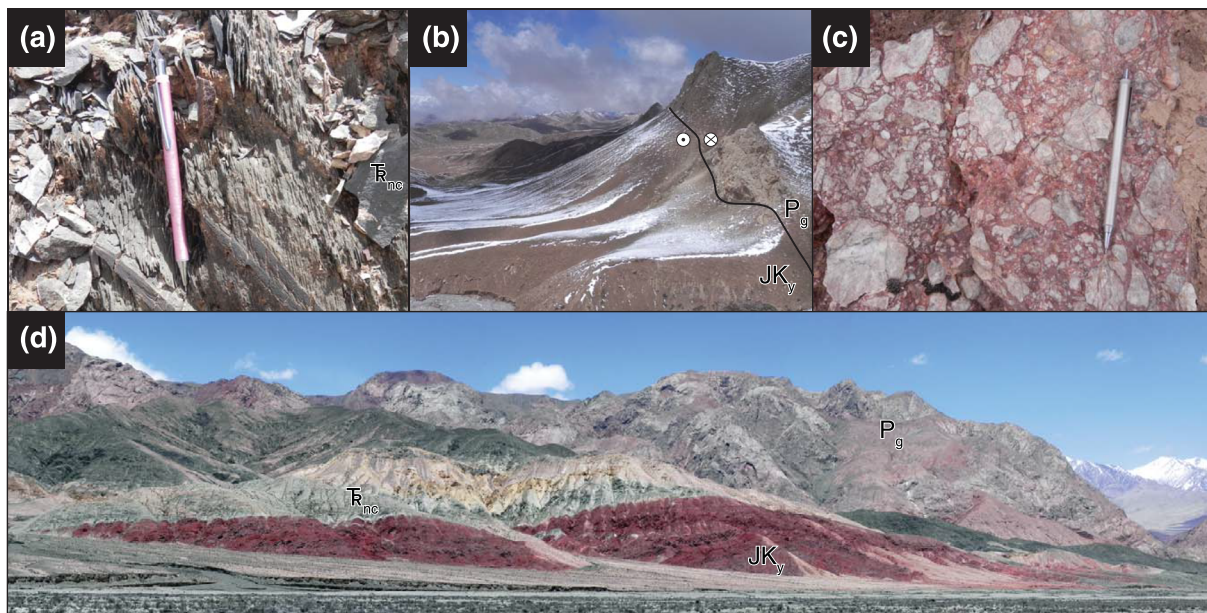


Figure 5. Field photographs of structural features observed. (a) Axial planar cleavage developed in shale layers and tilted sandstone bedding within the Triassic Naocangjiangou Group. (b) Westward looking photo of a large strike-slip fault along the northern Dongdatan Valley, with friable Triassic strata to the south (left) and steep topography developed within the Permian carbonate units to the north (right). (c) Well-developed breccia along the same fault shown in (b). (d) Taken looking roughly northeast and shows a well-defined thrust fault with Triassic metapelites thrust over upper Yangqu Group red bed strata.

the Permian Ganjia and Maerzheng Groups have been thrust over Triassic metapelites (Figures 2a and 3; Qinghai Bureau of Geology and Mineral Resources [QBGMR], 1980, 1981). This fault relationship is best exposed on either side of the Dongdatan Valley, along the northern East Wenquan Basin and as a series of small klippen in a tectonic sliver immediately north of the Wenquan Reservoir (Figures 2a and 3). Deformed Triassic Naocangjiangou metapelites preserve tight east-west oriented folds and near-vertical axial planar cleavage (Figure 5a), suggesting that the maximum compressive stress was oriented north-south, in modern coordinates, and the least compressive stress was oriented vertically during the episode of deformation preserved in these strata. Based on field observations and the degree of tilting preserved in the strata, the contractional strain preserved in Jurassic to Cenozoic sedimentary units is far less than in the Triassic Naocangjiangou. Thus, major shortening of the Triassic strata took place prior to deposition of the Yangqu Group and perhaps before deposition of the Triassic Babaoshan Group. In the central East Wenquan Basin, Cenozoic red beds are typically mildly tilted and overlie the Triassic Naocangjiangou Group in angular unconformity (Figure 4f), with the exception of red bed exposures near strike-slip faults that are locally strongly deformed. North of the Wenquan Reservoir, the Wenquan Hu thrust fault has been eroded on either side and is preserved as a klippe (Figures 2a and 3) that places Triassic metapelites over Jurassic–Cretaceous Yangqu Group (Figure 5d).

2.2.2. Left-Lateral Shear

The Kunlun fault zone deforms a broad region within the central East Kunlun Shan, such that left-lateral faulting is pervasive within the study area. Major faults identified include the Xidatan fault (the Xidatan-Dongdatan segment from van der Woerd et al., 2002), which is the main strand of the Kunlun fault east of the Kunlun Pass, and the Middle Kunlun fault, which delineates a major structural boundary between Proterozoic and Triassic strata in the eastern portion of the field area (Figures 1 and 2b; Kidd et al., 1988; Qinghai Bureau of Geology and Mineral Resources [QBGMR], 1980, 1981). The mountainous terrane north of the Dongdatan Valley is crosscut by left-lateral faults that are subordinate to the main Xidatan fault (Figure 2a). Subordinate faults offset Permian–Cenozoic strata, form well-defined gouge and fault rock zones, and tend to produce steep, near-vertical, topography when exposed in the Permian carbonate units (Figures 5b and 5c). Few minor strike-slip faults are exposed along the southern Dongdatan Valley (Figure 2a).

Where the Xidatan fault crosscuts the East Deshuiwai Mountains, to the east of Dongdatan Valley, it has created a wide fault gouge zone, up to hundreds of meters in thickness, and forms a major structural

discontinuity that separates Triassic metapelites to the north from Permian carbonate to the south (Figure 2b; Qinghai Bureau of Geology and Mineral Resources [QBGM], 1980, 1981). Within the East Deshuiwai Mountains, left-lateral faulting is accommodated over a broad network of multiple strike-slip faults. The Xidatan fault and subordinate faults occasionally carry small fault bound blocks of allochthonous Permian carbonates that are isolated within a separate lithologic unit (Qinghai Bureau of Geology and Mineral Resources [QBGM], 1980, 1981). The southern boundary of the East Deshuiwai Mountains is a strike-slip fault, here named the Da Lang fault (after a large wolf sighted nearby), which continues to the west into the East Wenquan Basin and eventually merges with the Xidatan fault (Figures 2a and 2b; Qinghai Bureau of Geology and Mineral Resources [QBGM], 1980, 1981).

2.2.3. Modern Fault Activity

Offset Quaternary alluvial strata along the Xidatan and Da Lang faults, along with active seismicity, suggests that strike-slip motion is presently accommodated within the central East Kunlun Shan (U.S. Geological Survey National Earthquake Information Center [USGS NEIC]). In the western and central portions of the field area, the surficial trace of the Xidatan fault is evident from pressure ridges and offset Quaternary fluvial and alluvial features and is occasionally associated with hot springs and sag ponds. Terrestrial cosmogenic nuclide dating of offset river terraces in Dongdatan Valley suggests that the Xidatan fault has accommodated $10\text{--}11\text{ mm yr}^{-1}$ of Late Pleistocene–recent left-lateral motion (van der Woerd et al., 1998, 2002). Modern seismic data also suggest that faults within the East Deshuiwai Mountains are active (USGS NEIC). Slip rates along the Middle Kunlun fault and subordinate strike-slip faults have not been quantified, and seismic data do not provide evidence for modern fault activity (USGS NEIC). We found no compelling field evidence for recent faulting along the Middle Kunlun fault in the mapping area, suggesting that it may not be a major active structure.

3. Low-Temperature Thermochronologic Data

The timing of fault initiation can be derived from thermochronologic methods in extensional or contractional deformation regimes, where tectonic activity generates topographic relief and a local increase in erosion rate (Braun, 2005; Ehlers & Farley, 2003). Conversely, thermochronologic studies along strike-slip faults are relatively few since strike-slip faulting typically results in the lateral translation of fault blocks rather than vertical exhumation. Certain strike-slip fault geometries, however, are capable of producing vertical exhumation of sufficient magnitude to be recorded by low-temperature thermochronology, such as near fault junctions, terminations, and splays, as well as within restraining bends and along nonvertical fault planes (Benowitz et al., 2011; Duvall et al., 2013; Niemi et al., 2013; Spotila et al., 1998, 2001, 2007). We targeted these types of structural environments within the central East Kunlun Shan to constrain the timing of strike-slip fault motion. In order to constrain the timing of thrust faulting, on the other hand, we were required to avoid locations in which strike slip-related deformation had caused considerable exhumation. We therefore also targeted sampling sites in which clear thrust fault relationships exist and where we observed strike slip-related exhumation to be absent or negligible (Figure 1).

3.1. Sample Collection and Preparation

Bedrock samples were collected from apatite and zircon bearing rock types, including volcanic and plutonic rocks of andesitic-dacitic composition (Table 1). We also collected medium to coarse-grained sandstones that may have experienced sufficient burial to reset the apatite and zircon thermochronologic system prior to more recent fault-related exhumation. The limited topographic relief and heterogeneous geologic setting of our study site limited our ability to collect steep elevation transects, so we dated single samples to constrain the time of exhumation through the apatite (U-Th)/He, apatite fission track (AFT), and zircon (U-Th)/He effective closure temperatures. Sample locations and descriptions are available in Table 1.

Once collected, samples were crushed and sieved using standard laboratory procedures. Apatite and zircon crystals were separated from the bulk sample using standard density and magnetic techniques. Crystals were handpicked at the University of Michigan to ensure grain quality using standard procedures (Farley & Stockli, 2002; Reiners & Farley, 2001). For (U-Th)/He analyses, apatite and zircon crystals were individually analyzed for He content at the University of Michigan Helium Laboratory following procedures in Niemi and Clark (2017). Apatites for (U-Th)/He dating were analyzed for U, Th, and Sm content at the University of Arizona Radiogenic Helium Dating Laboratory, and zircons for (U-Th)/He dating were

Table 1

Sample Locations, Rock Type, Mean Apatite and Zircon (U-Th)/He Ages, and Pooled Apatite Fission Track Ages for Samples Collected From the Central Kunlun Shan

Sample	Unit and rock type	Sample location			Apatite (U-Th)/He (Ma)	Apatite fission track (Ma)	Zircon (U-Th)/He (Ma)
		Latitude (°)	Longitude (°)	Elevation (m)			
<i>Xidatan fault block</i>							
11UMT53	Tr ³ _{Bd} , granitic gneiss	35.7490	95.0279	4,241	19.22 ± 2.05	19.04 ± 2.21	39.63 ± 2.75
<i>Wenquan Hu thrust fault hanging wall</i>							
11UMT63	Xγδ, granodioritic gneiss	35.7630	95.2880	4,124	25.42 ± 2.85	—	—
12DDT07	Tr _{nc} , granitic gneiss	35.7740	95.3305	4,026	63.02 ± 7.06 ^a	—	—
12DDT09	Tr _{nc} , gneiss	35.7626	95.2999	4,068	33.58 ± 3.01	46.97 ± 5.07	98.14 ± 20.06 ^b
12DDT10	Tr _{nc} , gneiss	35.7680	95.2556	3,946	29.32 ± 3.64	52.00 ± 4.84	72.50 ± 9.24
12DDT24	Tr _{nc} , gneiss	35.7523	95.2014	4,063	30.33 ± 1.69	43.04 ± 3.80	—
<i>Wenquan Hu thrust fault footwall</i>							
11UMT56	JK _y , sandstone	35.7563	95.2258	4,046	21.45 ± 3.73	43.22 ± 4.42	256.61 ± 59.27 ^b
<i>East Deshuiwai Mountains restraining bend</i>							
13DDT008	Tr ³ _b , metavolcanic	35.8779	95.7872	4,542	148.27 ± 47.13 ^c	—	—
13DDT009	Tr ³ _b , arkose	35.8714	95.7877	4,558	137.13 ± 107.52 ^c	—	—
<i>Deshuiwai Basin</i>							
13DDT016	Tr ³ _b , arkose	35.8255	96.4173	3,929	49.48 ± 9.53 ^a	—	—
13DDT022	Tr ² _{Yg} , granodiorite	35.8880	96.4496	4,123	35.42 ± 6.67 ^a	96.47 ± 14.88	—
13DDT032	PL, andesitic dike	35.9095	96.1664	4,752	36.42 ± 7.07	114.89 ± 12.93	—
<i>Other samples</i>							
12DDT17	JK _y , volcanic	35.7639	95.2836	4,084	37.38 ± 6.02 ^b	—	140.04 ± 12.43
12DDT22	Tr ³ _b , sandstone	35.9404	95.2364	4,691	38.30 ± 9.96 ^b	—	97.05 ± 11.62
13DDT011	P _m , metavolcanic	35.6320	96.2459	4,916	31.84 ± 4.13	64.43 ± 12.77	—
13DDT017	Tr _{nc} , tonalitic intrusion	35.6688	96.0487	4,373	75.76 ± 25.72 ^a	—	—
13DDT021	Tr ² _{Yg} , granitoid float	35.8880	96.4496	4,123	50.75 ± 7.05	—	—
13DDT023	Tr ² _{Yg} , granodiorite	35.8708	96.4514	4,053	54.13 ± 15.63 ^b	—	—
13DDT036	P ¹ _L , granite	35.9126	96.3012	4,538	73.13 ± 42.75 ^b	—	—

Note. All uncertainties are standard deviation reported at 1σ.

^aIndicates correlation between the AHe age and eU (correlation coefficient >0.85), possibly resided within PRZ for some time. ^bHelium analyses exhibit poor reproducibility (standard deviation >20%) that cannot be attributed to age-eU or age-grain size correlations. ^cIndicates correlation between AHe age and grain size (correlation coefficient >0.99), possibly resided within PRZ.

analyzed for U and Th content at the University of Colorado Thermochronology Research and Instrumentation Laboratory. AFT analyses were completed for one sample (12DDT10) at the University of Cincinnati and for seven other samples at the University of Arizona. Mounts of apatite grains were etched in 5 M HNO₃ solution (5.5 M for 12DDT10) at 21°C for 20 s to expose tracks from spontaneous fission of ²³⁸U. Following neutron irradiation at the Oregon State TRIGA Reactor, mica external detectors were etched in 40% HF at 20°C for 45 min (40 min for 12DDT10) to reveal induced tracks.

3.2. Apatite (U-Th)/He Age Results

We collected and dated 19 bedrock samples for apatite (U-Th)/He thermochronology with a minimum of four apatite single-grain replicates analyzed per sample. Measured AHe ages range widely across the central East Kunlun Shan, with mean ages between 20 and 148 Ma (Table 1 and supporting information Table S1). Two samples, 13DDT23 and 13DDT36, were removed from further analysis because the standard deviation of replicate apatite ages exceeded 20%, indicating that the mean ages for these samples are not well constrained (Table 1). Five other samples exhibit correlations between age and effective Uranium content (eU) or grain size (Samples 12DDT07, 13DDT008, 13DDT009, 13DDT016, and 13DDT017; Figures S1 and S2). In the following paragraphs, we describe the results and geologic setting for samples from west to east.

We collected nine bedrock samples from Dongdutan Valley and the East Wenquan Basin. The westernmost sample, 11UMT53, was collected from a small plutonic body that intruded the Triassic Naocangjiangou Group prior to metamorphism. This sample had an AHe age of 19.2 ± 2.1 Ma (Figure 2a and Table 1). To the east, Samples 12DDT24, 12DDT10, 11UMT63, 12DDT09, and 12DDT07 were collected from small plutonic bodies within the hanging wall of the Wenquan Hu thrust fault (Figures 2a, 3, and 5d and Table 1).

The AHe ages for these samples range between 25 and 33 Ma, with the exception of 12DDT07, which was dated at 63.0 ± 7.1 Ma (Table 1). Sample 12DDT07 shows a strong correlation between eU content and AHe age (Table S1 and Figure S1), the implications of which are discussed below.

From the footwall of the Wenquan Hu thrust fault, Samples 11UMT56 (sandstone) and 12DDT17 (interbedded tephra) were collected from the Yangqu Group strata. The mean AHe age for Sample 11UMT56 is 21.5 ± 3.7 Ma, and the mean AHe age for Sample 12DDT17 is 37.4 ± 6.0 Ma (Figures 2a and 3 and Table 1). In the northwestern corner of the East Wenquan Basin, Sample 12DDT22 was collected from the upper Triassic Babaoshan Group and provides an AHe age of 38.3 ± 10.0 Ma (Figure 2a and Table 1). Sample 12DDT22 was collected ~2 km to the north of the surface exposure of the Middle Kunlun fault (Figure 2a).

Within the East Deshuiwai Mountains, we collected Samples 13DDT008 and 13DDT009 from interbedded volcanic and metamorphosed arkosic sandstone layers, respectively, of the Triassic Naocangjiangou Group. The replicate AHe ages from 13DDT008 range between 86 and 201 Ma, and the replicate ages from Sample 13DDT009 range between 16 and 309 Ma (Figure 2b and Table 1). Apatite replicates for Samples 13DDT008 and 13DDT009 show a strong correlation between AHe age and crystal size, suggesting slow cooling (Figure S2; Reiners & Farley, 2001). To the southeast of the East Deshuiwai Mountains, Sample 13DDT017, collected from a small plutonic body that intrudes into the Triassic Naocangjiangou Group, displays a strong correlation between age and eU. Within the East Deshuiwai Mountains, Sample 13DDT011 was collected from a metamorphosed volcanic unit and provides an AHe age of 31.8 ± 4.1 Ma (Figure 2b and Table 1). This region of the East Deshuiwai Mountains is strongly deformed due to strike-slip motion and largely composed of Permian marine carbonate, such that exposed apatite-bearing rock types are scarce.

To the north of the Deshuiwai Basin, we collected several igneous samples that intrude the Proterozoic Wanbaoguo Group. Apatite quality was poor and only one sample (13DDT032) provided reproducible AHe ages. Sample 13DDT032 was collected from an andesitic dike and provides a mean AHe age of 36.4 ± 7.1 (Figure 2b and Table 1). Within the center of the Deshuiwai Basin, the Triassic Babaoshan and Jurassic–Cretaceous Yangqu Group are fairly undeformed and well exposed. We collected a bedrock sample from an arkosic sandstone of the Babaoshan Group (13DDT016), which provided an AHe age of 49.5 ± 9.5 Ma (Figure 2b and Table 1). This sample shows a correlation between eU and replicate age (Figure S1), similar to Samples 13DDT017 and 12DDT07. Nearby, to the northeast, several plutonic units of lower Triassic age are exposed (Figure 2b; Qinghai Bureau of Geology and Mineral Resources [QBGMR], 1980, 1981). We collected two samples, 13DDT022 and 13DDT023, from these large intrusions of andesitic-dacitic composition. Sample 13DDT022 was dated using AHe analysis at 35.4 ± 6.7 Ma and 13DDT023 has very poor replicate agreement and was omitted from further analysis (Tables 1 and S1).

3.3. Apatite Fission-Track Age Results

We selected eight samples for AFT analysis (Figures 2a and 3 and Tables 1 and S2) and analyzed between 12 and 23 apatite grains for each sample. Samples with fewer than 20 analyzed apatite crystals suffered from mediocre apatite yield (11UMT56, 13DDT011, and 13DDT022). All samples passed the χ^2 -test, suggesting that all grains from each sample are representatives of a single age population (Table S2; Galbraith, 1981). Track density was insufficient for track length analyses in most mounted samples aside from Sample 12DDT09, from which we measured a mean confined track length of 13.93 ± 0.20 μm ($n = 13$).

The AFT age for the westernmost sample (11UMT53) is within uncertainty of the apatite (U-Th)/He age, at 19.0 ± 2.2 Ma (Figures 2a and 3 and Table 1). To the east, AFT ages for Samples 11UMT56 and 12DDT24 are within uncertainty of each other at 43.2 ± 4.4 and 43.0 ± 3.8 Ma, respectively (Figures 2a and 3 and Table 1). Near the Wenquan Reservoir, AFT ages for Samples 12DDT09 and 12DDT10 are 47.0 ± 5.1 and 52.0 ± 4.8 Ma, respectively, and within uncertainty of each other (Figures 2a and 3 and Table 1). Between the Xidatan and Da Lang fault strands, Sample 13DDT011 was dated at 64.4 ± 12.8 Ma (Figure 2b and Table 1). We obtained Cretaceous AFT ages of 114.9 ± 12.9 Ma for Sample 13DDT032 and 96.5 ± 14.9 Ma for Sample 13DDT022 collected from the Deshuiwai Basin (Figure 2b; Table 1).

3.4. Zircon (U-Th)/He Age Results

We obtained zircon (U-Th)/He (ZHe) ages for 6 of the 19 samples collected for thermochronologic analysis (Figures 2a and 3 and Table 1). We dated a minimum of three zircon crystals per sample (Table S3). All

samples had reproducible ZHe ages with standard deviation of replicate zircon ages less than 20% of the mean age (Tables 1 and S3).

The zircon (U-Th)/He age for the westernmost sample collected for thermochronologic analysis (11UMT53) provided an Eocene age of 39.6 ± 2.8 Ma (Figures 2a and 3 and Table 1). To the east, Samples 12DDT09 and 12DDT10 were collected from the hanging wall of the Wenquan Hu thrust fault and have ZHe ages of 98.1 ± 20.1 and 72.5 ± 9.2 Ma, respectively (Figures 2a and 3 and Table 1). Samples 11UMT56 and 12DDT17 in the footwall of the Wenquan Hu thrust fault were dated using ZHe analysis at 256.6 ± 59.3 and 140.0 ± 12.4 Ma, respectively (Figures 2a and 3 and Table 1). We collected Sample 12DDT22 from the northern East Wenquan Basin, from which we obtained a ZHe age of 97.1 ± 11.6 Ma (Figure 2a and Table 1).

4. Low-Temperature Thermochronology Modeling and Implications

4.1. Implications for the Timing of Red Bed Deposition in the Dongdatan Valley

The age of strata in the footwall of the Wenquan Hu thrust fault provides an important constraint for thermal modeling and interpretations of local and regional faulting. While previous mapping suggests that the footwall strata are Paleocene–Neogene, our thermochronologic data suggest otherwise. The mean ZHe ages attained from the footwall Samples 11UMT56 and 12DDT17 are over 100 Ma apart, and 11UMT56 displays considerable scatter. Furthermore, our zircon He ages from 11UMT56 are older than the youngest detrital U-Pb zircon ages and generally overlap with a major 200–280 Ma detrital U-Pb age populations from the same strata (McRivette et al., 2019; Wu, Zuza, Zhuo, et al., 2019). From this, we suggest that the red bed strata in the footwall of the Wenquan Hu thrust fault was not buried to sufficient depth to reset the zircon He system, such that the ages from 11UMT56 represent detrital zircon cooling ages. Furthermore, the 140 Ma zircon (U-Th)/He age from 12DDT17 is much younger than the ~245 Ma maximum depositional age from detrital U-Pb data (McRivette et al., 2019) and thus represents syndepositional volcanic tephra ages. Given the Cretaceous ZHe age for Sample 12DDT17, we suggest that these strata are not Cenozoic, as previously mapped, but are rather part of the Jurassic–late Cretaceous Yangqu Group. Since the ZHe ages do not inform us about the cooling history of the footwall fault block, they are excluded from QTQt modeling, below.

4.2. Thermal Modeling Results

In order to quantify the timing and rate of cooling of different fault blocks in the central East Kunlun Shan, we used QTQt version 5.5.1c, a program for modeling low-temperature thermochronology that employs a Bayesian transdimensional Markov chain Monte Carlo inversion scheme (Gallagher, 2012). For most thermal models, we grouped multiple samples to model fault blocks because QTQt is particularly useful for handling large data sets. For models with multiple samples, we allowed the temperature offset between samples to vary over time and input sample elevations to inform the model of modern temperature offset. The fault blocks modeled include a block proximal to the Xidatan fault and the East Deshuiwai Mountains restraining bend to constrain the timing of strike slip-related exhumation, the Wenquan Hu thrust fault hanging wall and footwall to constrain the timing of thrust fault-related exhumation, and the Deshuiwai Basin to constrain the cooling history in the eastern study region and discern whether the Middle Kunlun fault has caused recent exhumation (Figure 6). A list of samples, types of thermochronologic data, geologic constraints, reasoning for geologic constraints, and general priors for each fault block modeled is provided in Table 2.

For every model, we ran 10^4 burn-in trials and 10^5 postburn-in trials, the latter of which are retained for analysis. Additionally, we inspected the posterior iteration chain to ensure that trials had sufficiently sampled the parameter space. We placed minimal geologic constraints on our models to avoid forcing the results to any preconceived prior assumptions. We require that every model reached surface temperatures (0–20°C) by 0 Ma. For the Wenquan Hu footwall block, we required the model to be near-surface temperatures (0–20°C) during a broadly defined depositional age of the Yangqu Group (170–50 Ma). In order to assess whether a model fit well or if additional parameters and constraints needed adjustment, we compared predicted and observed thermochronologic ages for mean sample ages and individual grain ages (Figure 7).

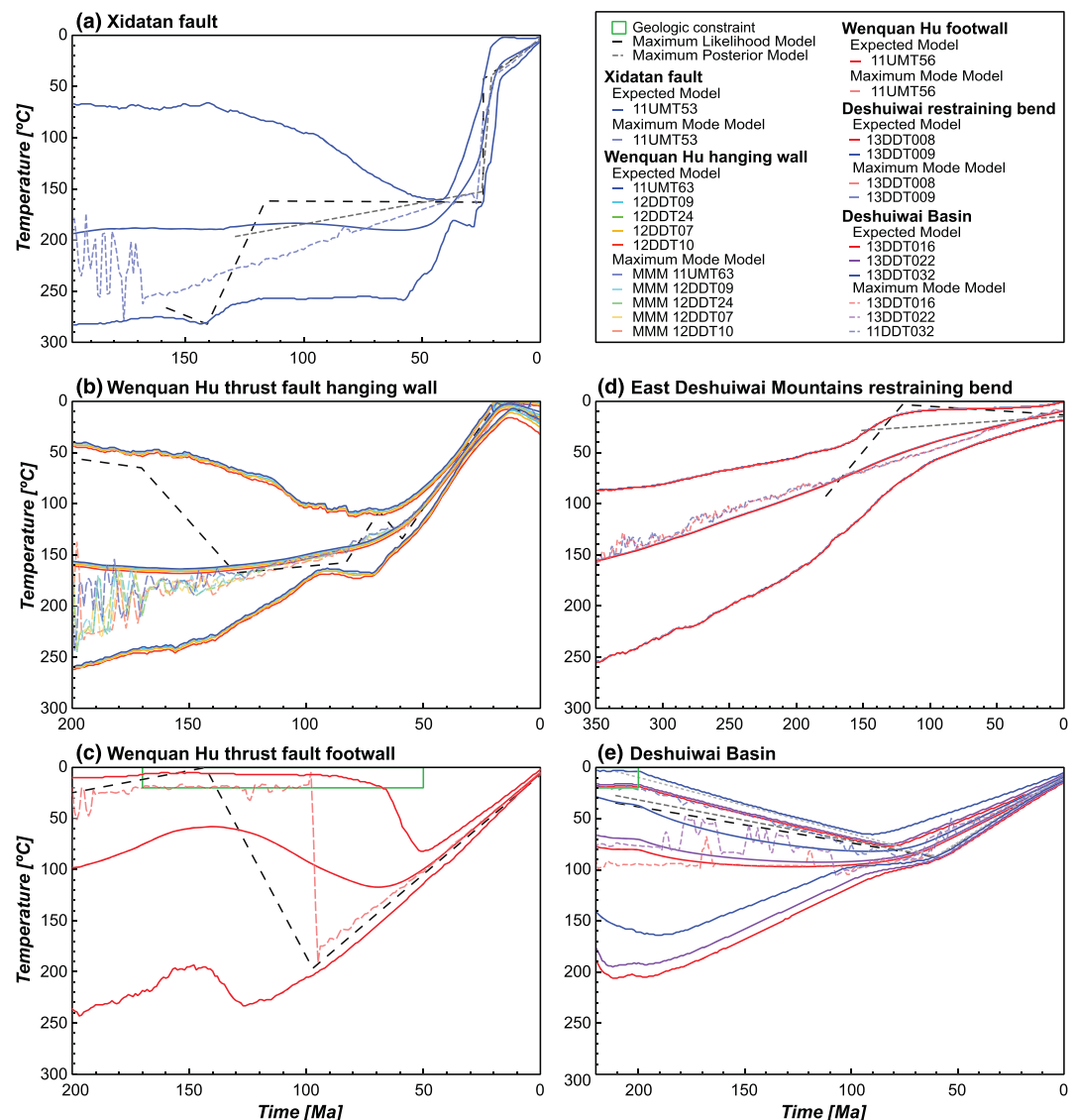


Figure 6. QTQt modeling (Gallagher, 2012) results of thermochronologic data from various fault blocks in the central East Kunlun Shan. (a) Model results for crustal exhumation proximal to the Xidatan fault. (b) Model results for exhumation of the hanging wall of the Wenquan Hu thrust fault. (c) Model results for burial and exhumation of the footwall of the Wenquan Hu thrust fault. Green box represents the geologic constraint for deposition at surface temperatures of the Yangqu Group. (d) Model results for exhumation of the East Deshuiwai Mountains, a restraining bend along the Xidatan fault zone. (e) Model results for the Deshuiwai Basin, with a geologic constraint for deposition at surface temperatures of the Babaoshan Group.

4.2.1. Xidatan Fault Model Results

To model cooling of the Xidatan section of the Kunlun fault and constrain the timing of strike-slip faulting related exhumation, we used a single sample collected from a small intrusive body near the trace of the main fault strand (Figure 2a). Sample 11UMT53 was collected in a region for which expected exhumation due to strike-slip faulting is expected based on the high relief of the landscape associated with pervasive strike-slip fault zones (Figure 1). The apatite (U-Th)/He and fission track ages are within uncertainty of each other, and the zircon (U-Th)/He ages are the youngest in our data set (Table 1). Our QTQt model results show a broad swath of possible time-temperature paths prior to 55 Ma, with best fit model results showing isothermal holding, followed by an acceleration in cooling that likely initiated between 55 and 40 Ma (Figure 6a). This early Cenozoic stage of cooling is not required by all models but is preferred by the Maximum

Table 2
QTQt Thermochronologic Modeling Inputs and Reasoning

Fault block	Samples	Thermochronologic data input	Geologic constraint	Supporting observation	Range for general prior
Xidatan fault	11UMT53	AHe, AFT, ZHe ages	0–20°C by 0 Ma; maximum cooling rate 1000°C/Myr	Sample collected from gneiss body (small pluton intruded into Triassic Naocangjianguo Group) directly north of the Xidatan fault in Dongdatan Valley. All thermochronologic ages appear reset.	0–300°C and 0–300 Ma
Wenquan Hu thrust fault hanging wall	11UMT63 12DDT07 12DDT09 12DDT10 12DDT24	AHe, AFT, ZHe ages; AFT track lengths	0–20°C by 0 Ma; maximum cooling rate 1000°C/Myr	Samples collected from metamorphosed plutonic bodies emplaced within the Triassic Naocangjianguo Group in the hanging wall of the Wenquan Hu thrust fault. All thermochronologic ages appear reset.	0–300°C and 0–300 Ma
Wenquan Hu thrust fault footwall	11UMT56 12DDT17	AHe, AFT ages	0–20°C at 170–50 Ma; 0–20°C by 0 Ma; maximum cooling rate 1000°C/Myr	Samples collected from the Yangqu Group strata in the footwall of the Wenquan Hu thrust fault. AHe and AFT ages appear reset. ZHe ages are interpreted as either detrital ages (11UMT56) or volcanic emplacement ages (12DDT17). Terrestrial deposition, at surface temperatures, loosely constrained between middle to late Jurassic and Eocene time.	0–300°C and 0–300 Ma
East Deshuiwai Mountains restraining bend	13DDT008 13DDT009	AHe ages	0–20°C by 0 Ma; maximum cooling rate 1000°C/Myr	Samples collected from the restraining bend between Wenquan and Deshuiwai Basins. Both samples show significant scatter in ages and correlation between AHe age and apatite grain size, suggesting slow cooling and variable He diffusion.	0–300°C and 0–300 Ma
Deshuiwai Basin	13DDT016 13DDT022 13DDT032	AHe, AFT ages	0–20°C at 250–200 Ma; 0–20°C by 0 Ma; maximum cooling rate 1000°C/Myr	Samples collected from Triassic sedimentary and igneous in the East Deshuiwai Basin. Sample 13DDT16 collected from the upper Triassic Babaoshan Group. Terrestrial deposition, at surface temperatures, constrained during upper Triassic time.	0–300°C and 0–300 Ma

Likelihood and Maximum Posterior models (Figure 6a; MLM and MPM). Rapid cooling of 20.0–21.6°C Myr^{−1} initiated circa 23 Ma, followed by a deceleration in cooling rate by circa 17 Ma (Figure 6a). The modeled and observed thermochronologic ages are in general agreement with each other, with (U-Th)/He mean predicted and observed ages within uncertainty of each other (Figure 7a). However, models were unable to reproduce the young AFT age (Figure 7a). Despite the difficulty in modeling overlapping AHe and AFT ages, the similarity in these ages qualitatively requires rapid exhumation at this time.

4.2.2. Wenquan Hu Thrust Fault Hanging Wall Model Results

For our QTQt model for the hanging wall of the Wenquan Hu thrust fault, we used five samples with apatite (U-Th)/He, AFT, and zircon (U-Th)/He ages to constrain time-temperature paths. Samples were collected from a klippe exposed near Wenquan Reservoir (Figure 3), in a region where exhumation due to strike-slip faulting is not observed (Figure 1). Model results show slow to moderate cooling rates over Mesozoic time. Cooling rates accelerated by 50–65 Ma and remained elevated for roughly until 19–21 Ma (Figure 6b), followed by slow to negligible cooling from the Miocene to present time.

Predicted mean thermochronologic ages are generally in good agreement with observed data, with the notable exception of Sample 12DDT07 (Figure 7e). This sample shows a strong correlation between effective uranium and apatite (U-Th)/He age (Figure S1), suggesting that ages may be influenced by radiation damage in the apatite crystals that accumulated during a period of isothermal holding. Isothermal holding and the accumulated radiation damage may have occurred at an earlier period in time, possibly Cretaceous given the observed ages, thus inhibiting our ability to discern the Cenozoic cooling history from Sample

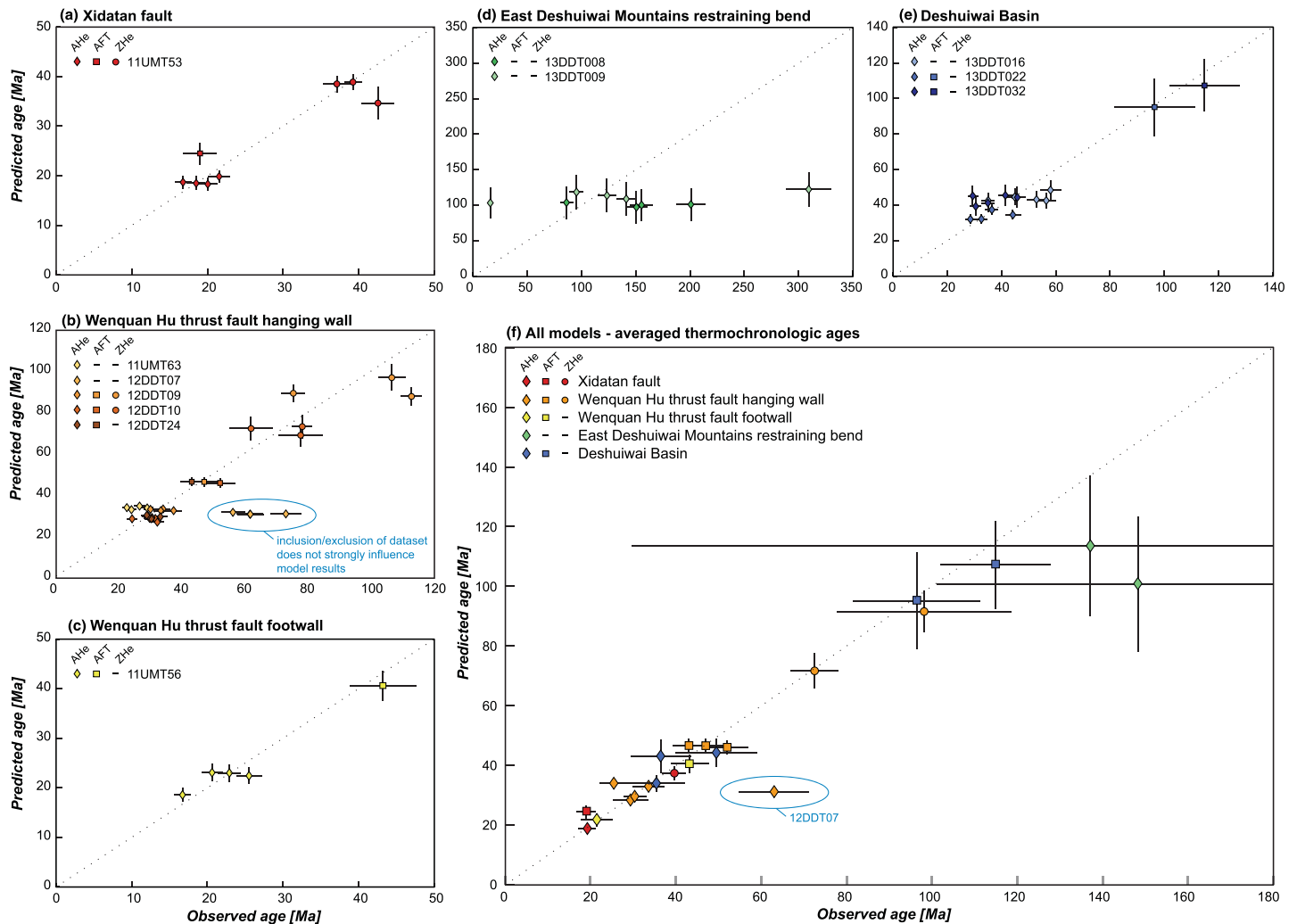


Figure 7. Observed and predicted thermochronologic ages for best fit QTQt models shown in Figure 6. Plots show age and 1σ uncertainty, as well as a dashed 1:1 line to assess goodness of fit. Apatite fission track ages and individual apatite and zircon (U-Th)/He aliquot ages for modeling time-temperature paths (a) near the Xidatan fault, (b) in the Wenquan Hu thrust fault hanging wall block, (c) in the Wenquan Hu footwall fault block, (d) in the East Deshuiwai Mountains restraining bend, and (e) in Deshuiwai Basin. (f) Mean observed and modeled ages are calculated from the individual ages shown in Figures 7a–7e for each sample modeled in all fault blocks. Modeling results for the Wenquan Hu hanging wall block are nearly identical whether 12DDT07 is included or excluded from QTQt. Despite ~20% uncertainty in 12DDT09 the mean zircon (U-Th)/He age, inclusion of these data improves the model fit to all other observed samples. Abbreviations include AHe = apatite (U-Th)/He, AFT = apatite fission track, and ZHe = zircon (U-Th)/He.

12DDT07. The possible existence of microinclusions is another potential explanation for the unusually old observed ages in 12DDT07. We modeled the Wenquan Hu hanging wall both with and without 12DDT07 ages and found that model results are agnostic to this sample. Selecting the RDAAM radiation damage model (Flowers et al., 2009) in QTQt did not improve the fit to Sample 12DDT07. In our thermal model, we also included zircon (U-Th)/He ages from Sample 12DDT10, despite the scatter in individual grain ages. Inclusion of these ages results in a better fit to all other thermochronologic data (Figure 7b), and model results are also capable of matching the mean observed zircon (U-Th)/He ages for 12DDT10.

While our mean observed and predicted ages show good agreement, some of the individual modeled and observed AHe grain ages do not agree well (Figure 7b). This is likely a result of combining multiple samples into a single thermal model of the entire fault block. To investigate this further, we modeled each sample individually in QTQt. We found that differences between observed and predicted individual grain ages

are reduced when each sample is modeled separately; however, the QTQt algorithm simplifies the time-temperature paths for each sample, as these are constrained by fewer data points (Figure S3). Nonetheless, the individually modeled sample runs show significant overlap in preferred time-temperature paths, suggesting a common exhumation history. Indeed, we find that the modeled time-temperature histories for individually modeled samples are within uncertainty of the predicted time-temperature paths modeled using all samples together (Figure S3). We therefore suggest that modeling the samples together is advantageous and informative about the exhumation history experienced by all hanging wall samples, despite having slightly diminished goodness of fit to individual AHe ages.

4.2.3. Wenquan Hu Thrust Fault Footwall Model Results

We used two samples collected from the Wenquan Hu thrust fault footwall strata (11UMT56 and 12DDT17) to constrain the timing of burial due to thrust faulting and subsequent regional exhumation. Samples were collected in a region where significant exhumation due to strike-slip faulting is not expected (Figure 1). Our model included a surface temperature constraint for the depositional age of the terrestrial Yangqu sedimentary strata, forcing time-temperature paths to pass through $10 \pm 10^\circ\text{C}$ from 170–50 Ma (Figure 6c). Since the samples were collected several kilometers from each other (Figure 3), we allowed the initial temperature offset to vary within $20 \pm 20^\circ\text{C}$ but required that the temperature offset converge to more similar values by modern time.

Model results show a range of possible time-temperature paths prior to circa 65 Ma, after which time model results show with heating from near-surface temperatures. Heating is followed by moderate, monotonic cooling rates to surface temperatures initiating by 50 Ma. Predicted thermochronologic ages for model results agree well with the observed ages (Figures 7c and 7f). Based on the similarity of AFT ages in the hanging wall and footwall (Table 1), we suggest that the Wenquan Hu thrust fault ceased motion by 43 Ma and that the hanging wall and footwall began to cool together after this time. This is supported by the similarity in post-43 Ma cooling rates for the hanging wall and footwall thermal models, where the average post-43 Ma cooling rate for the hanging wall and footwall models are 1.9 ± 0.3 and $2.0 \pm 0.3^\circ\text{C Myr}^{-1}$, respectively.

4.2.4. East Deshuiwai Mountains Restraining Bend Model Results

We modeled the time-temperature paths for the East Deshuiwai Mountains, which is a restraining bend between the East Wenquan and Deshuiwai basins, to constrain the timing of strike slip-related exhumation (Figures 1 and 2b). For this model, we included apatite (U-Th)/He ages from Samples 13DDT008 and 13DDT009. Apatite ages from these samples display significant scatter between 16 and 309 Ma (Table 1). These samples were collected from the Triassic-age Babaoshan unit, and thus the apatite (U-Th)/He ages appear to record partial resetting of the (U-Th)/He systematics arising from postdepositional exhumation of the region. Both samples also show a strong correlation between crystal size and age (Tables 1 and S1). Grain size-age correlations are often associated with isothermal holding in the partial retention zone followed by rapid uplift (Reiners & Farley, 2001). Model results show generally slow cooling over Mesozoic–present time, with a possible brief increase in cooling rate between 160–120 Ma (Figure 6d). Unfortunately, predicted model ages do not agree well with observed apatite (U-Th)/He ages (Figure 7d). Qualitative assessment of sample ages from the East Deshuiwai Mountain may provide some assessment on the timing of exhumation within the restraining bend, as discussed below, but detailed cooling information is not resolved by inverse thermal modeling of these samples, likely due to the wide spread in observed grain ages.

4.2.5. Deshuiwai Basin and Middle Kunlun Fault Model Results

We used apatite (U-Th)/He and fission track ages from Samples 13DDT016, 13DDT022, and 13DDT032 to model time-temperature paths in QTQt for the Deshuiwai Basin and the Middle Kunlun fault (Figure 2b). The goal of this modeling approach was to constrain the timing and rate of regional cooling of the Deshuiwai Basin, where we do not observe field evidence for exhumation due to motion on Cenozoic structures (Figure 1). The range immediately north of the Middle Kunlun fault, on the other hand, may have a history of exhumation separate from the Deshuiwai Basin (Figure 1). We tested whether or not faulting along the Middle Kunlun fault caused significant exhumation north of Deshuiwai Basin by dating Sample 13DDT032. The apatite (U-Th)/He and fission track results from 13DDT032 are within uncertainty of ages from 13DDT022 (Tables 1, S1, and S2) and are collected on the other side of the Middle Kunlun fault (Figure 2b), suggesting that both samples have experienced similar cooling histories since mid-Cretaceous time. Thus, we used all three samples in QTQt to model the cooling history of the Deshuiwai Basin and

Table 3
Fault Gouge Data From Thrust and Strike-Slip Faults Sampled in the Dongdatan Valley

Sample	Size fraction (μm)	$^{40}\text{Ar}/^{39}\text{Ar}$ age (Ma)	Proportion $2M_1$ (%)	F-recoil (%)
11UMT50	1.0–2.0	119.76 ± 0.52	37 ± 4	17.2
	0.5–1.0	117.62 ± 0.71	27 ± 4	15.0
	0.2–0.5	104.58 ± 0.39	15 ± 4	18.8
	0.05–0.2	93.75 ± 0.33	5 ± 4	21.9
11UMT52	1.0–2.0	168.77 ± 1.17	85 ± 4	10.1
	0.5–1.0	172.92 ± 0.78	78 ± 4	8.1
	0.2–0.5	163.05 ± 0.45	42 ± 4	10.1
	0.05–0.2	131.30 ± 0.41	36 ± 4	24.6
11UMT52	1.0–2.0	72.17 ± 0.40	55 ± 4	14.8
	0.5–1.0	80.09 ± 0.59	42 ± 4	13.0
	0.2–0.5	69.86 ± 0.61	30 ± 4	15.5
	0.05–0.2	54.65 ± 0.21	10 ± 4	21.7
12DDT18	1.0–2.0	142.39 ± 0.87	45 ± 4	20.3
	0.5–1.0	172.61 ± 0.64	37 ± 4	11.9
	0.2–0.5	132.52 ± 0.50	10 ± 4	21.6
	<0.05	117.35 ± 0.53	4 ± 4	23.7

mountains immediately to the north (Figure 6e). Since Sample 13DDT016 was collected from the terrestrial Triassic Babaoshan Group, we added constraint that cooling paths are preferred to pass through $10 \pm 10^\circ\text{C}$ from 250–200 Ma (Table 2). Model results show slow burial starting in the Triassic. Burial and heating continued until ~90 Ma, possibly lasting until 60–50 Ma, followed by monotonic cooling to the present (Figure 6e). We ran a similar model without Sample 13DDT032, which was collected north of the Middle Kunlun fault zone, and found no major difference in the modeled cooling history.

For the Deshuiwai Basin and Middle Kunlun fault models, predicted apatite (U-Th)/He and AFT mean ages are in general agreement with observed ages (Figures 7e and 7f). Slow cooling rates since Cretaceous or early Eocene time is in agreement with field observations that the Yangqu and Babaoshan Groups are flat-lying to mildly tilted but otherwise relatively undeformed in the Deshuiwai Basin (Figures 4a and 4b). The degree of tilting and deformation of Mesozoic terrestrial strata increases near the Middle Kunlun fault; however, the similarity in cooling histories on either side of the fault indicates that either deformation occurred before the mid-Cretaceous or that exhumation due to strike-slip faulting along the Middle Kunlun fault did not result in significant vertical exhumation.

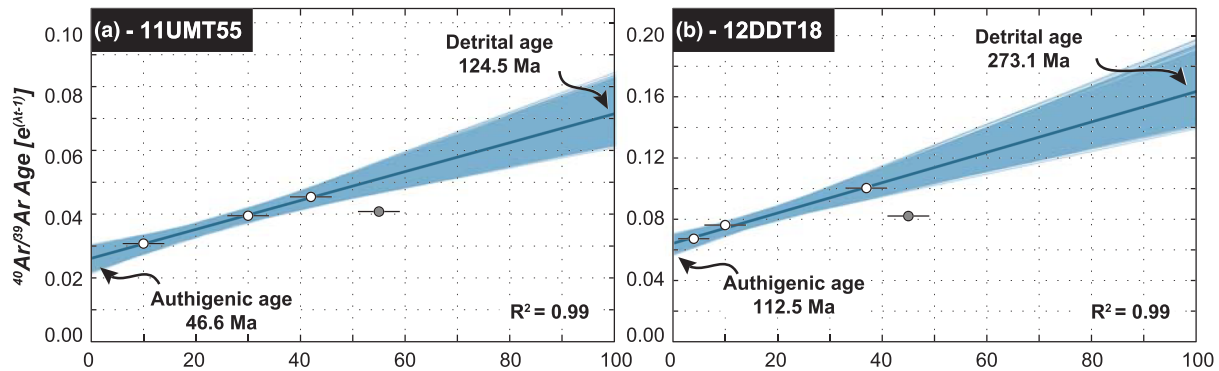
5. $^{40}\text{Ar}/^{39}\text{Ar}$ Fault Gouge Dating

Fault gouge, formed along fault surfaces during discrete events of fault slip as wall rock undergoes brittle deformation, contains clay-sized minerals that are well suited for age dating, such as potassium-bearing illite (van der Pluijm et al., 2001). Authigenically grown illite (polytype $1M_d$) is a diagenetic product of tectonic activity and is a common target for fault gouge dating (van der Pluijm et al., 2001). Separation of pure authigenic illite from detrital illite (polytype $2M_1$) is not usually possible in fault gouge material because of the fine grain size of these clays and similar density and settling properties, and so authigenic and detrital illite ages are typically estimated from a two-end-member mixing model derived from $^{40}\text{Ar}/^{39}\text{Ar}$ ages determined on mixtures with differing fractions of each polytype (van der Pluijm et al., 2001). The authigenic illite age is often interpreted to record the timing of faulting, whereas the detrital illite age corresponds to an inherited component reflecting the time of regional illite growth or the timing of metamorphism (van der Pluijm et al., 2001). Authigenic illite can, however, grow under a variety of conditions, such as during regional low-temperature metamorphism (Verdel et al., 2012), and thus interpretation of fault gouge ages requires careful consideration of independent records of regional tectonic and metamorphic history. Several recent analyses of combined thermochronologic and fault gouge dating highlight the potential power of using multiple independent chronometers to constrain the timing of upper crustal brittle deformation (Duvall et al., 2011; Staisch et al., 2016).

5.1. Sample Collection and Preparation

We collected fault gouge samples from thrust and strike-slip faults throughout the Dongdatan Valley, East Wenquan Basin, and East Deshuiwai Mountains by identifying fault zones with clay rich gouge material. Because authigenic illite crystals tends to be smaller than detrital illite crystals (Grathoff & Moore, 1996), aliquots in which the relative proportion of each illite polytype varied were created by gravitational separation in a centrifuge. We measured each sample aliquot on a Scintag X1 Powder X-Ray Diffractometer (PXRD) at the University of Michigan Electron Microbeam Analysis Laboratory (EMAL). The relative abundance of detrital and authigenic illite was estimated by comparing standard $2M_1$ and $1M_d$ powder patterns to measured patterns. The error of polytype pattern matching is generally between 3% and 5% (Haines & van der Pluijm, 2008), and we assume a $\pm 4\%$ error for the mixing fraction of each aliquot. Aliquots were analyzed for $^{40}\text{Ar}/^{39}\text{Ar}$ geochronology at the University of Michigan Argon Geochronology Laboratory. For illite age analysis, the total gas ages are used to determine the age of the illite polytype mixtures present in each

Thrust Faults



Strike-Slip Faults

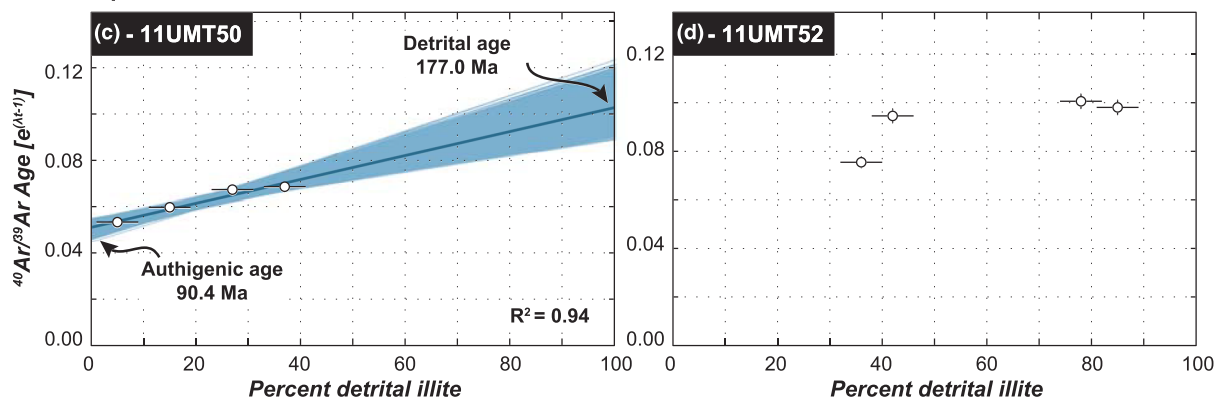


Figure 8. Results for fault gouge dating within the Dongdatan Valley. For each sample, size fraction aliquot age and illite concentrations are plotted as small dots. Age errors are present but hidden by the size of data points. Data points that are used for authigenic illite age estimation are shown as white dots, and data points omitted are shown as gray dots. The best fit results from Bayesian linear regression are shown as dark blue lines, and other acceptable linear regression lines are shown in lighter blue. (a) Thrust fault Sample 11UMT55 with an estimated fault gouge age of 46.6 Ma. (b) Thrust fault Sample 12DDT18 with an estimated fault gouge age of 112.5 Ma. (c) Strike-slip fault Sample 11UMT50 with an estimated fault gouge age of 90.4 Ma. (d) Strike-slip fault Sample 11UMT52 with no estimate for the timing of fault motion due to lack of linear age-illite concentration trend.

aliquot. We assumed an uncertainty in of 3% for the $^{40}\text{Ar}/^{39}\text{Ar}$ age of each aliquot in order to account for external errors (Dazé et al., 2003; Karner & Renne, 1998; Renne et al., 1998).

Possible natural loss of ^{40}Ar was assessed by examining the fraction of ^{39}Ar recoil during irradiation for each sample aliquot (f-recoil; Table 3), which is a proxy for illite crystallinity (Dong et al., 1995). Finally, the authigenic and detrital ages are estimated using the same Bayesian linear regression method employed by Staisch et al. (2016), in which the error in polytype concentration and geochronologic age are propagated into the uncertainty of the extrapolated end-member ages (Figure 6). The modeled linear regression with the highest likelihood of fitting the observed data was deemed the best fit line, from which we calculated the estimated authigenic and detrital illite ages for each sample. We report errors in slope and intercept values at the 2σ level. An expanded description of fault gouge illite age analysis methodology is in supporting information Text S1.

5.2. $^{40}\text{Ar}/^{39}\text{Ar}$ Fault Gouge Dating Results

The X-ray diffractometer (XRD) powder patterns and modeled illite mixtures for each aliquot are available in Figures S4–S7, $^{40}\text{Ar}/^{39}\text{Ar}$ age spectra are plotted in Figures S8–S11, and Ar release data are available in Table S4. The simplified results for each sample aliquot are in Table 3 and plotted in Figure 8. In the following sections, we discuss the results and interpretations of the fault gouge geochronologic data.

5.2.1. Thrust Fault Gouge Ages

The two fault gouge samples from thrust faults (11UMT55 and 12DDT18) were collected from similar structural settings in which Triassic metapelites are thrust over the Jurassic–Cretaceous Yangqu Group along the Wenquan Hu thrust fault (Figure 2a). Under the assumption that authigenically grown illite is younger than

the formation age of detrital illite within the surrounding wall rock, and given that that authigenic illite grains tend to be smaller than detrital grains, we expect younger $^{40}\text{Ar}/^{39}\text{Ar}$ ages in smaller size fraction aliquots (van der Pluijm et al., 2001). However, in both thrust fault gouge samples collected from Dongdatan Valley, we do not see a well-defined relationship between the aliquot ages and authigenic illite proportions. Samples 11UMT55 and 12DDT18 display a linear age-illite polytype fraction relationship in the three finest size fractions measured, but the coarsest size fraction in both samples deviates from this trend and is younger than the next coarsest size fraction (Figure 8; Table 3). In both samples, we see an increase in f-recoil measured in the coarsest size fraction compared to the next largest size fraction, which likely corresponds to a decrease in illite crystallinity (Figure S12, Table 3, and Text S1). On this basis we suggest that apparent total gas ages measured for the coarse size fractions are erroneously young. Thus, we omit the coarsest size fraction for both thrust fault gouge samples and analyze the remaining three finest size fractions to determine an age of authigenic illite growth (Figure 8). The Bayesian linear regression for Sample 11UMT55 produces an authigenic illite age of 46.6 ± 4.0 Ma, a detrital illite age of 124.5 ± 11.3 Ma, and an R^2 value of 0.99 (Figure 8a). Using a similar regression scheme, Sample 12DDT18 produces a fault gouge age of 112.5 ± 5.8 Ma, a detrital illite age of 273.1 ± 27.4 Ma, and an R^2 of 0.99 (Figure 8b).

5.2.2. Strike-Slip Faults

Samples 11UMT50 and 11UMT52 were collected from recently or currently active strike-slip faults located to the north and south of the Dongdatan Valley, respectively. Only Sample 11UMT50 provides an interpretable age-illite concentration pattern. Sample 11UMT52 has a nonlinear relationship between illite concentration and $^{40}\text{Ar}/^{39}\text{Ar}$ age, and the deviation from the expected linear trend cannot be explained by the measured f-recoil. We therefore suggest that the $^{40}\text{Ar}/^{39}\text{Ar}$ age data from Sample 11UMT52 cannot be interpreted using a two-end-member mixing model. Fault gouge ages from Sample 11UMT50 do show a correlation between $^{40}\text{Ar}/^{39}\text{Ar}$ age and detrital illite component. The Bayesian linear regression through this fault gouge data suggests that the authigenic illite component was formed at 90.4 ± 4.7 Ma and that the detrital illite has an age of 177.0 ± 16.4 Ma. The best fit regression has an R^2 value of 0.95 (Figure 8c).

6. Discussion

In this work, the thermochronologic and geochronologic data presented from the central East Kunlun Shan, along the northern margin of the Tibetan Plateau, record the timing, rate, and magnitude of upper crustal exhumation and fault activity over the past several tens of millions of years. In concert with detailed geologic mapping that characterizes the structural position of these thermochronologic samples, we can resolve the timing of major changes in structural style, and thus potentially stress orientation, throughout the Cenozoic evolution of the Tibetan Plateau. The structural evolution and shift in stress accommodation is a promising avenue for understanding the attainment of high elevation throughout the orogen and complimentary to more paleoaltimetric data. Thus, we will interpret thermochronologic and structural data in light of several fundamental tectonic questions with respect to the northern plateau margin, specifically, and the evolution of high topography throughout the Tibetan Plateau, more generally.

In the following section, we constrain the deformation history of the East Kunlun Shan by exploring the structural and exhumation histories from (1) regions that have evidence for Cenozoic thrust faulting but have not been subject to significant cooling following the onset of major lateral shear as well as (2) regions that appear to be dominated by recent strike-slip fault deformation and exhumation. We then integrate this tectonic history into a broader perspective of the evolution of the Tibetan Plateau and discuss how changes in structural style along the northern plateau margin may reflect the evolution of stress state of the Tibetan Plateau, as a proxy for the attainment of high elevation and gravitational potential energy. Furthermore, the spatiotemporal details of structural changes may provide insight into the geodynamic mechanisms responsible for elevation gain.

6.1. The Timing of Crustal Shortening

The East Wenquan Basin was formed in part as an extensional step over between the Xidatan and Middle Kunlun faults and forms a topographic low in the central East Kunlun Shan (Figure 1). As a region of strike-slip fault-related subsidence, it is more likely to preserve an older record of thrust fault-related exhumation and cooling, such as along the Wenquan Hu thrust fault (Figures 2 and 3). QTQt modeling of the Wenquan Hu thrust fault hanging wall shows slow cooling over the majority of the Mesozoic followed by

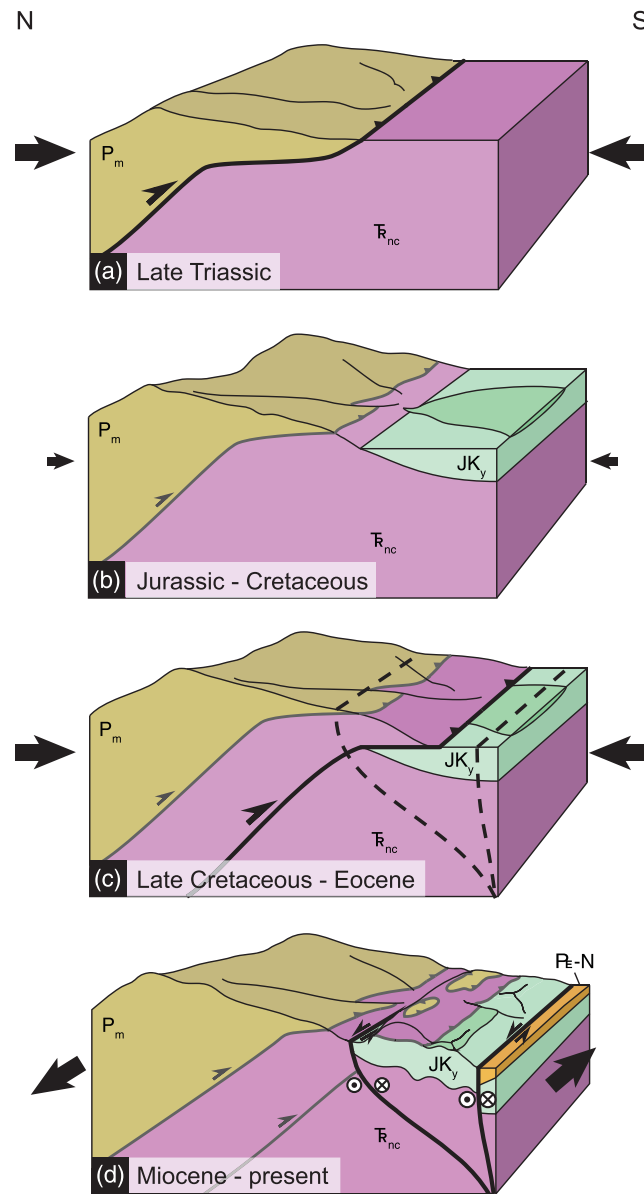


Figure 9. Schematic block diagrams showing the evolution of deformation within the Dongdatan Valley. (a) Field observations of Permian carbonates thrust over Triassic metapelites and regional dating of plutons and metamorphic cooling episodes (Liu et al., 2005; Mock et al., 1999; Wu, Zuza, Chen, et al., 2019) suggest that the East Kunlun Shan experienced late Triassic north-south oriented compression from the northward accretion of the Qiangtang block. (b) North-south compression may have been reactivated during Jurassic–Cretaceous accretion of the Lhasa block based on the timing of Yangqu Group deposition and a separate regional cooling event documented in the West and East Kunlun Shan (Li et al., 2019; Liu et al., 2005). Permian marbles and Triassic metapelites were exposed at the time of Yangqu deposition. (c) Late Cretaceous to Eocene shortening from collision between India and Eurasia resulted in thrust faulting along the Wenquan Hu thrust fault and burial of terrestrial strata in the footwall. Shortening and exhumation may have continued elsewhere in the East Kunlun Shan into late Eocene time but ceased along the Wenquan Hu thrust fault by 43 Ma. (d) East-west oriented strike-slip faulting locally causes exhumation and erosion. Thermochronologic modeling suggest that strike-slip faulting initiated by ~20 Ma. Miocene–present strike-slip faulting results in basin subsidence in the East Wenquan basin, deposition of terrestrial strata, and juxtaposition of Jurassic–Cretaceous and Cenozoic strata.

an increase in exhumation as early as 50–65 Ma, coincident with burial in the footwall (Figures 6b and 6c). The similarity of AFT ages and post-43 Ma cooling rates on either side of the Wenquan Hu thrust fault suggests that motion along this structure had ceased by 43 Ma and that the hanging wall and footwall blocks were subsequently exhumed together (Figures 6b and 6c). We interpret thermochronologic data

and models to indicate a period of crustal shortening along the Wenquan Hu thrust fault between Paleocene and early Eocene time (Figure 9c). Post-43 Ma cooling rates may be due to a combination of regional uplift along other tectonic structures, discussed below, and surface processes.

Illite age analyses of fault gouge collected from the Wenquan Hu thrust fault yield authigenic illite ages of 47 and 113 Ma from two different samples collected along strike (Figures 8a and 8b). The Eocene fault gouge age determined for the westernmost sample overlaps with the timing of crustal shortening inferred from our thermochronologic modeling. The Cretaceous age for the easternmost fault gouge sample, on the other hand, coincides with a time of slow to negligible cooling in the hanging wall (Figure 6b). We suggest that the 113 Ma authigenic illite age from the easternmost sample is an inherited age from either ^{40}Ar loss during Cretaceous low-grade metamorphism, which can produce a similar age-size fraction relationship as expected for fault-related authigenic illite growth (Verdel et al., 2012), or from an earlier phase of shear deformation as inferred from $^{40}\text{Ar}/^{39}\text{Ar}$ dating of nearby shear zones (Arnaud et al., 2003). The inherited age indicates that the site of our eastern fault gouge sample may not have been suitable for authigenic illite growth during Eocene thrust faulting along the Wenquan Hu thrust fault, possibly due to a lack of circulating hot fluids or other environmental parameters that stimulate authigenic illite growth.

While our thermochronologic modeling suggests that shortening accommodated on the Wenquan Hu thrust fault ceased by 43 Ma, previous studies show that crustal shortening and resultant exhumation continued elsewhere in the central East Kunlun Shan into late Eocene time and possibly into late Oligocene time (Figure 9c). For example, thermochronologic data and modeling in the East Kunlun Shan shows initial rapid exhumation as early as 40–41 Ma (Mock et al., 1999; Shi et al., 2018; Wang et al., 2017), and modeling of apatite (U-Th)/He ages from the southern margin of the Qaidam Basin show unroofing initiating around 35 Ma (Clark et al., 2010). Clark et al. (2010) suggest that shortening and exhumation continued along the Kunlun-Qaidam Basin margin due to motion along the South Qaidam fault until at least 24 Ma. Exhumation along the South Qaidam fault may have caused uplift and cooling in our study area and may thus be a component of Eocene–early Miocene cooling modeled across the Wenquan Hu thrust fault and in the East Deshuiwai Basin (Figure 6). Taken together, these data from northern Tibet suggest that shortening initiated in Paleocene to early Eocene time in the south central East Kunlun Shan such that the modern northern margin was established early in the Indo-Asian collision history and that shortening-related exhumation continued farther north along Kunlun-Qaidam Basin margin into the middle Miocene (Clark et al., 2010; Duvall et al., 2011; Yin et al., 2002).

6.2. The Onset of Left-Lateral Shear

In the western Dongdatan Valley, thermochronologic ages from a Triassic gneiss collected within 1 km of the Xidatan fault yield ~19 Ma cooling ages from both apatite (U-Th)/He and fission track methods (Figure 2a). According to experimental and field studies of transpressional environments, exhumation due to strike-slip faulting is commonly of high magnitude and highly localized near the fault trace (Malusà & Fitzgerald, 2019; Niemi et al., 2013; Spotila et al., 2001; Wilcox et al., 1973). Thermal modeling of our data indicates rapid cooling between $20.0^\circ\text{C Myr}^{-1}$ and $21.6^\circ\text{C Myr}^{-1}$ in the interval between 23 and 17 Ma (Figure 6a). Near the Kunlun Pass, thermochronologic ages collected along the Kunlun fault are similarly young, with AHe ages between 8 and 17 Ma and ZHe ages between 8 and 29 Ma (Figure 1; Duvall et al., 2013). Importantly, the Miocene episode of rapid cooling is only captured in thermochronologic data sets collected near the Kunlun and Xidatan faults and is not apparent in data sets collected distal from strike-slip faulting. Thus, we interpret Miocene rapid cooling to be caused by localized exhumation along strike-slip faults.

Thermochronologic data from the East Deshuiwai Mountains, a restraining bend along the Xidatan fault zone (Figure 1), suggest post–early Miocene exhumation related to strike-slip faulting. While thermal modeling results from Samples 13DDT008 and 13DDT009 are not able to clearly determine the cooling histories recorded in either sample (Figures 6d and 7d), apatite (U-Th)/He data show a strong correlation between measured age and crystal sizes (Figure S2). A similar relationship has been recognized in the Big Horn Mountains in the United States and has been shown to suggest exhumation of a partial retention zone and that the youngest age can be used as a maximum time prior to exhumation (Reiners & Farley, 2001). Thus, we suggest that these rocks were isothermally held for upward of 100 Myr and that cooling increased after ~16 Ma, the youngest age measured in these samples, due to transpressional shear. Prolonged

isothermal holding is in agreement with thermochronologic modeling of Clark et al. (2010) and our QTQt modeling throughout the region (Figure 6). However, this interpretation is based on a single crystal age, and we stress that this model should be considered with caution. Taken together, our thermochronologic data and thermal modeling from the Dongdatan Valley and East Deshuiwai Mountains suggest that strike-slip faulting initiated as early as 23 Ma and that transpression-related exhumation is highly localized near the trace of the Xidatan fault and within restraining bends.

Illite age analysis of fault gouge collected from a shear zone north of the Dongdatan Valley does not record Miocene strike-slip fault activity but rather a mid-Cretaceous authigenic illite age. The absence of young illite age populations may suggest that the environment along sampled strike-slip faults is not conducive to authigenic illite growth or that there has been insufficient transpressional exhumation such that any Miocene or younger authigenic illite produced at depth has not been brought to the surface. The Cretaceous authigenic illite age may be remnant from low-grade metamorphism and ^{40}Ar loss in nature (Verdel et al., 2012) or an earlier phase of mid-Cretaceous deformation (Arnaud et al., 2003). Regardless of genesis, fault gouge ages from material sampled along strike-slip faults in our field area do not provide meaning for data to constraining the onset of lateral shear in the East Kunlun Shan.

Based on thermochronologic ages and structural observations from the Dongdatan Valley and East Deshuiwai Mountains, we suggest that left-lateral faulting within the East Kunlun Shan initiated by 20 Ma and possibly as early as 23 Ma. This is in agreement with an increase in the cooling rate between 20 and 15 Ma inferred from thermochronologic data farther to the west along the Kunlun fault (Duvall et al., 2013). Thermochronologic data from Duvall et al. (2013) may also record an earlier phase of cooling that initiated between 30 and 25 Ma and continued until 20–15 Ma. This period overlaps with the period of inferred crustal shortening (Clark et al., 2010) as well as our inferred onset of strike-slip faulting by 23–20 Ma in the East Kunlun Shan. Model results from Duvall et al. (2013) are constrained by apatite and zircon (U-Th)/He ages that are similar to our ages collected near the Xidatan fault; however, our inclusion of AFT data allow our model to define a discrete 23–20 Ma interval of cooling along the Xidatan fault. Thus, we suggest that Duvall et al. (2013) age results are produced from the same period of transpression along the Kunlun fault but that their lack of AFT age constraints lead to a more broadly defined period of cooling.

6.3. Deformation History Throughout the Tibetan Plateau and Implications for Surface Uplift

A main goal of this study was to constrain the timing of the transition in mode of deformation, from shortening to shear, in the central East Kunlun Shan and to relate this transition to broader geodynamic implications for the evolution of the Tibetan Plateau. We integrate our new structural, thermochronologic, and geochronologic data sets with previous work from throughout Tibet to obtain a spatial and temporal framework for the kinematic and topographic evolution of the orogen.

6.3.1. Early Cenozoic Crustal Shortening

Prior to the Indo-Asian collision, the northern Tibetan Plateau was a major depocenter for material eroded from an Andean-type margin, which stretched from the Gangdese batholith in the south to the Tanggula Shan in the north (McRivette et al., 2019; Staisch et al., 2014). During or soon after the ~50–60 Ma Indo-Asian collision, it has been inferred that crustal shortening stepped north of the Tanggula Shan to the modern northern plateau margin at the southern edge of the Qaidam Basin (Clark et al., 2010; Dupont-Nivet et al., 2010; Duvall et al., 2011, 2013; Molnar & Stock, 2009; Najman et al., 2010; Rowley, 1996; Staisch et al., 2016; Yin et al., 2002, 2008). Our new mapping, thermochronologic modeling, and fault gouge dating in the East Kunlun Shan are consistent with the inference of northward stepping of the plateau margin near the time of collision.

Strong lithospheric blocks to the north of the East Kunlun Shan focused plateau growth to the south of the Qaidam Basin; thus, the majority of crustal shortening in northern Tibet from 50–35 Ma occurred between the Tanggula Shan and the Kunlun Shan (Figure 10a; Burg et al., 1983; Clark, 2012; Clark et al., 2010; DeCelles, Quade, et al., 2007; Ding et al., 2014; Duvall et al., 2011; England & Searle, 1986; Hetzel et al., 2011; Kapp, DeCelles, Gehrels, et al., 2007; Kapp, DeCelles, Leier, et al., 2007; Kapp et al., 2005; Lin et al., 2020; Murphy et al., 1997; Rohrmann et al., 2012; Yin et al., 2008). DeCelles et al. (2011) postulate that the Greater Indian lithosphere underthrust the Lhasa terrane early in the collision history, which may explain the propagation of crustal shortening north of the Tanggula Shan after the Indo-Asian collision, as well as a northward sweep in volcanism into the Qiangtang terrane (Figure 10a; Ding et al., 2003, 2007; Kapp

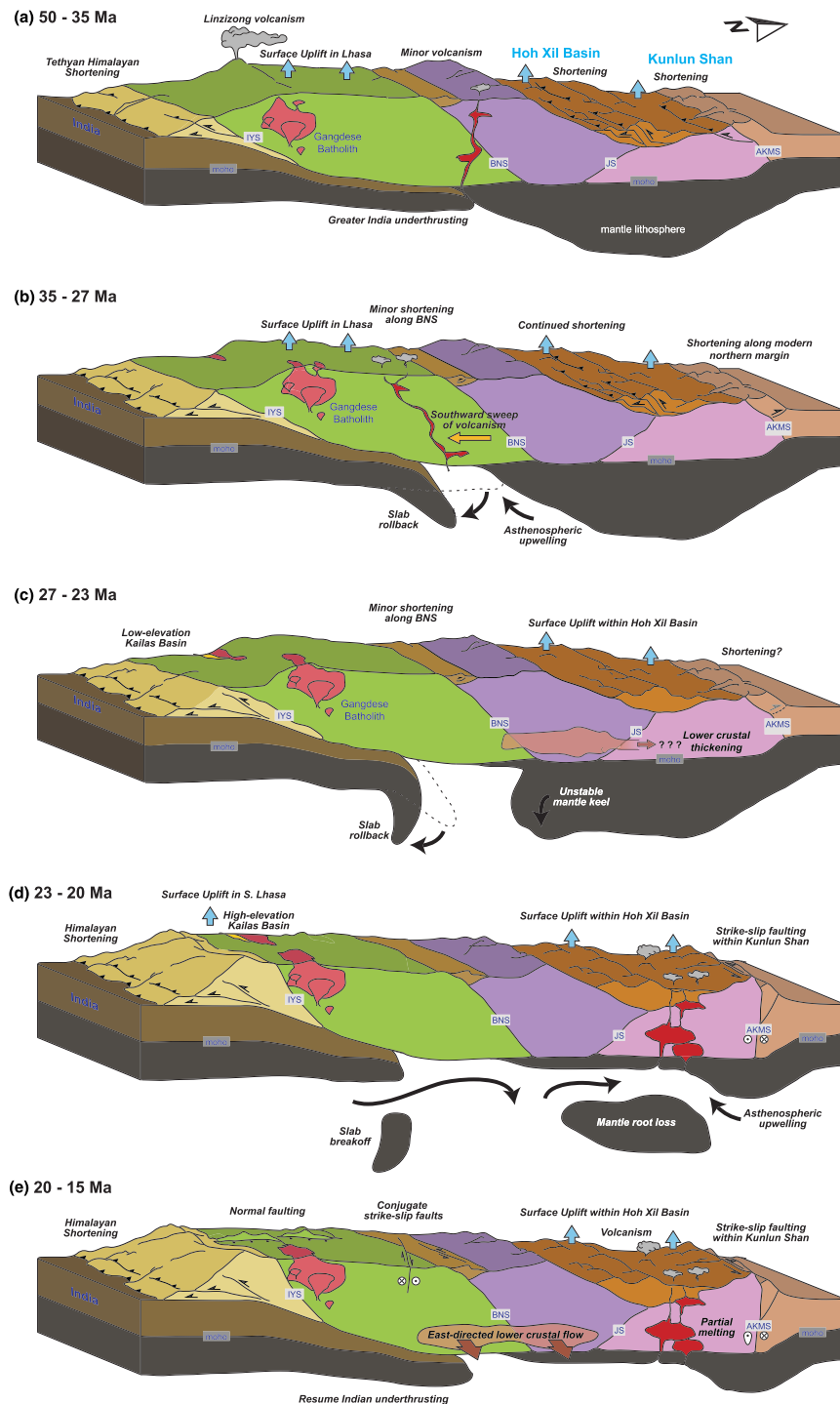


Figure 10. Schematic orogen-scale cross section of the geodynamic evolution of the Tibetan Plateau. (a) The onset of crustal shortening and thickening in northern Tibet soon after the Indo-Asian collision continued into late Oligocene time with moderate elevation gain. (b) Shortening in northern Tibet continues as a southward sweep of magmatism suggests the onset of slab rollback in southern Tibet. (c) Shortening ceases within the Hoh Xil Basin by 27 Ma and likely by 24 Ma in the East Kunlun Shan. Surface uplift may have continued due to crustal thickening via lower crustal flow in northern Tibet. Continued slab rollback may have destabilized the northern Tibetan mantle root by removing its southern buttress. (d) The onset of strike-slip faulting in the East Kunlun Shan between 23 and 20 Ma is coincident with proposed slab breakoff and elevation gain in southern Tibet and proposed mantle root loss, surface uplift, and increased magmatism within the northern Tibet. (e) After 20 Ma, strike-slip and normal faulting expanded throughout the Tibetan Plateau, coincident with the proposed onset of eastward directed lower crustal flow.

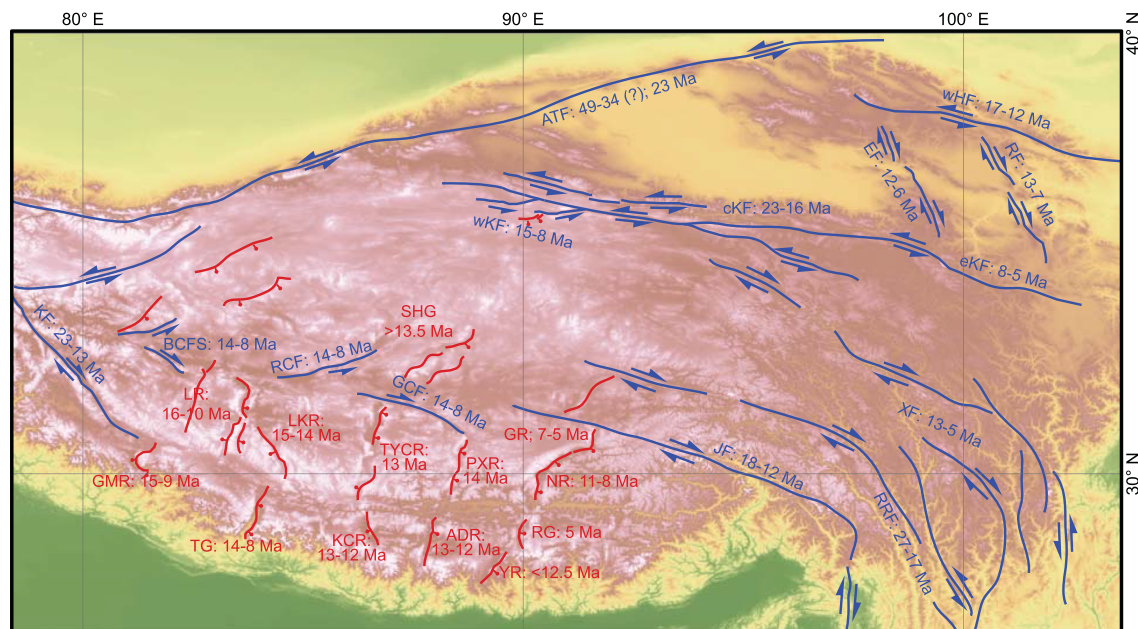


Figure 11. Map of major active strike-slip and normal faults in the Tibetan Plateau, adapted from Styron et al. (2010) and Fu et al. (2011). The estimated initiation age of each fault system is denoted, along with abbreviated names. Abbreviations for strike-slip faults are as follows: cKF = central Kunlun Fault, eKF = East Kunlun Fault, wKF = West Kunlun Fault, wHF = West Haiyuan Fault, EF = Elashan Fault, RF = Riyueshan Fault, ATF = Altyn Tagh Fault, JF = Jiali Fault, RRF = Red River Fault; KF = Karakoram Fault, XF = Xianshuihe Fault, RCF = Riganpei Co Fault, GCF = Gyaring Co Fault, BCFS = Bue Co Fault system. Abbreviations for normal faults are as follows: TG = Thakkola Graben, ADR = Ama Drime Rift, KCR = Kung Co Rift, GMR = Gurle Mandhata Rift, RG = Ringbung Graben, YR = Yadong Rift, LR = Lunggar Rift, NR = Nyainqentangliah Rift, LKR = Lopukangri Rift, TYCR = Tangra Yum Co Rift, PXR = Pumqu-Xainza Rift, GR = Gulu Rift, SHG = Shuang Hu Graben. Citations for the initiation of faulting are available in Tables S5 and S6.

et al., 2003, 2005; Lin et al., 2020; Miller et al., 1999; Nomade et al., 2004; Williams et al., 2001, 2004; Yakovlev et al., 2019).

High elevation may have been attained in the central Tibetan Plateau by Eocene–Oligocene time (DeCelles, Quade, et al., 2007; Ding et al., 2014; Polissar et al., 2009); however, low to moderate elevation persisted in the intervening Hoh Xil Basin from late Oligocene to early Miocene time (Polissar et al., 2009; Sun et al., 2015), as well as in the Kailas Basin of southern Tibet (DeCelles et al., 2011), suggesting that crustal shortening alone did not produce high elevation throughout the Tibetan Plateau (Staisch et al., 2016). In the Lhasa and Qiangtang terranes, the temporal coincidence of late Oligocene to early Miocene arc-parallel extension in southern Tibet and a southward sweep of volcanism from the Qiangtang to the Lhasa terranes has been interpreted to result from slab rollback beneath Tibet (Figures 10b and 10c; DeCelles et al., 2011; Yakovlev et al., 2019). This geodynamic model also provides a mechanism for the coeval cessation of deformation in northern Tibet, in that slab rollback would potentially relieve northern Tibet of its deep-seated southern buttress and lead to an eventual change in stress orientations throughout the plateau (Figure 10c).

6.3.2. Miocene Plateau-Wide Change in Faulting Style

Abundant evidence suggests that the Tibetan Plateau underwent a significant reorganization of faulting style following the late Oligocene–early Miocene cessation of crustal shortening in the northern Tibetan Plateau (Figures 10d and 10e). For example, the Kunlun and Altyn Tagh are major strike-slip faults that dominate the deformation field of northern Tibet. Pre-Miocene piercing points along the Altyn Tagh fault show a common magnitude of offset, indicating that the inception of strike slip likely occurred in late Oligocene–early Miocene time (Ritts et al., 2008; Yin et al., 2002; Yue et al., 2001, 2004). This overlaps with our interpretation of new thermochronologic data, which suggest that left-lateral motion along the Kunlun fault initiated as early as 23 Ma and may have propagated to the east and west by ~16–8 Ma (Figure 11; Duvall et al., 2013; Jolivet et al., 2003).

In addition to the Kunlun and Altyn Tagh faults in northern Tibet, strike-slip faults throughout in the Tibetan Plateau initiated in the Miocene. In the Qilian Shan, left-lateral motion along the Haiyuan fault initiated slightly after Kunlun fault activity, circa 17 Ma (Duvall et al., 2013). In the eastern Qilian Shan,

thermochronologic data, along with sediment accumulation rates, provenance, and stable isotope records, indicate that north-south shortening ceased by 20 Ma and transitioned to eastward directed plateau expansion by circa 13 Ma (Hough et al., 2011; Lease et al., 2011, 2012; Z. Wang et al., 2012). Within central and southern Tibet, strike-slip faulting initiated by ~18–13 Ma (Figure 11; Armijo et al., 1986, 1989; Lee et al., 2003; Murphy et al., 2000; Phillips et al., 2004; Taylor et al., 2003; Taylor & Peltzer, 2006; Wang et al., 2009). Normal faults throughout the southern Tibetan Plateau also appear to initiate in early to middle Miocene time (Figure 11; Blisniuk et al., 2001; Garzione et al., 2003; Lee et al., 2011; McCallister et al., 2013; Murphy et al., 2002; Ratschbacher et al., 2011; Styron et al., 2013; Sundell et al., 2013). The coeval onset of normal and strike-slip faulting may reflect a change in the stress state across the Tibetan Plateau.

6.3.3. Geodynamic Mechanisms Responsible for Elevation Gain and a Shift in Stress Accommodation

Recent work has suggested that stress reorganization throughout the Tibetan Plateau may be due to a shift in middle Miocene related to changes in Pacific-Eurasia plate convergence (Zhuang et al., 2018). However, early Miocene onset of normal and strike-slip faulting throughout the Tibetan Plateau and its coincidence with records of uplift to high elevation throughout the plateau (DeCelles, Kapp, et al., 2007; DeCelles, Quade, et al., 2007; Ding et al., 2014; Polissar et al., 2009; Rowley & Currie, 2006; Wu et al., 2008; Xu et al., 2013) and onset of eastward plateau expansion via lower crustal flow (Clark & Royden, 2000; Clark, House, et al., 2005; Ouimet et al., 2010; Royden et al., 1997) imply a regional mechanistic cause rather than one of distal plate reorganization. Furthermore, the onset of strike-slip faulting along the Kunlun and Altyn Tagh faults is ~5–8 Ma older than normal and strike-slip fault initiation in central and southern Tibet, which indicates that the mechanistic cause for stress reorganization was initially focused in the northern Tibetan Plateau.

The mechanism of Miocene elevation gain in northern Tibet is debated; however, post-Oligocene crustal thickening of the Hoh Xil Basin, possibly via lower crustal flow, likely contributed to elevation gain in northern Tibet (Staisch et al., 2016). Additionally, widespread post-30 Ma magmatism in the Hoh Xil Basin may be suggestive of mantle root loss, which could result in relatively rapid uplift of 1–3 km (Chen et al., 2012; Chung et al., 2005; Ding et al., 2003; England & Houseman, 1989; Guo et al., 2006; Jiang et al., 2006; Lai et al., 2003; McKenna & Walker, 1990; Molnar & Stock, 2009; Molnar et al., 1993; Wang et al., 2005; Williams et al., 2004; Yakovlev et al., 2019). We propose that the late Oligocene to early Miocene period of slab rollback may have primed the northern Tibetan mantle lithosphere for delamination and foundering in the Miocene (Figures 10c and 10d). Lower crustal flow may be a possible separate mechanism for post-Oligocene surface uplift as its occurrence is not excluded by mantle root loss (Staisch et al., 2016) and both mechanisms are supported by petrologic and geophysical data (Arnaud et al., 1992; Ding et al., 2003; Guo et al., 2006, 2014; C. Jiang et al., 2014; D. Jiang et al., 2008; Karplus et al., 2011; Klemperer, 2006; McKenna & Walker, 1990; Owens & Zandt, 1997; Turner et al., 1993, 1996; Q. Wang et al., 2012; Xia et al., 2011; Yang & Ding, 2013). Regardless of the mechanism, an increase in elevation in northern Tibet would affect the average of force per unit length throughout the orogen (Molnar & Stock, 2009), indicating that uplift need not occur simultaneously or of equal magnitude to produce a plateau-wide shift in gravitational potential energy. Given the temporal coincidence in elevation gain in northern Tibet and the shift in stress accommodation throughout the Tibetan Plateau between 23 and 16 Ma, we suggest that uplift to high elevation in northern Tibet resulted in the increase in average gravitational potential energy across the orogen and the plateau-wide inception of strike-slip and normal faulting activity within ~5–8 Ma of onset (Figures 10d and 10e).

7. Conclusions

Our data from the central East Kunlun Shan provide new constraints on the deformation history of the northern Tibetan Plateau margin. Results from thermochronologic ages and modeling, $^{40}\text{Ar}/^{39}\text{Ar}$ fault gouge dating and structural mapping suggest that north-south oriented crustal shortening initiated between 65 and 50 Ma and ceased within the Dongdatan Valley by 43 Ma. Previous data collected elsewhere in the central East Kunlun Shan broaden the timing of crustal shortening into late Oligocene time (Clark et al., 2010; Mock et al., 1999). Our thermochronologic modeling results suggest a 23–20 Ma phase of rapid cooling near the Xidatan segment of the Kunlun fault zone. We interpret the increased cooling rate to result from highly localized uplift along transpressional sections of the Kunlun fault. We suggest these ages to

represent the onset of strike-slip faulting in the central East Kunlun Shan, as they are slightly older but consistent with previous work on the timing of sinistral shear in the Kunlun Shan (Duvall et al., 2013; Jolivet et al., 2003).

The early to middle Miocene kinematic shift from north-south oriented pure shear to east-west oriented simple shear throughout the orogen was likely driven by an increase in gravitational potential energy. One potential mechanism for increasing gravitational potential energy and reorganizing crustal scale stress is the development of high topography in the northern Tibetan Plateau. Given the absence of shortening in northern Tibet after late Oligocene to early Miocene time (Staisch et al., 2016), elevation gain and increase in gravitational potential energy was likely due to lower crustal thickening or mantle lithospheric thinning. The roughly coeval onset of strike-slip and normal fault activity throughout the Tibetan Plateau (Blisniuk et al., 2001; Garzzone et al., 2003; Lee et al., 2003; Lee et al., 2011; McCallister et al., 2013; Murphy et al., 2000, 2002; Phillips et al., 2004; Ratschbacher et al., 2011; Styron et al., 2013; Sundell et al., 2013; Taylor & Peltzer, 2006; Wang et al., 2009) and eastward plateau expansion via lower crustal flow (Clark, Bush, et al., 2005; Clark, House, et al., 2005; Clark & Royden, 2000) suggest that peak elevations may have been reached by middle Miocene time.

Data Availability Statement

All data and supporting information data are cataloged and publicly available at the USGS ScienceBase repository (<https://doi.org/10.5066/P9F3DZYQ>).

Acknowledgments

This work was funded through National Science Foundation Continental Dynamics Grants EAR-0908711 and EAR-1211434 to Niemi and Clark, an National Science Foundation Graduate Research Fellowship awarded to Staisch, a Geological Society of America Graduate Student Research Award to Staisch, and two University of Michigan Turner Grants awarded to Staisch. We acknowledge National Natural Science Foundation of China Grant 40921120406 to An Zhisheng, which supported our Chinese colleagues at the Institute for Earth Environment and our joint fieldwork in the Tibetan Plateau. We thank Peter Molnar for his efforts in leading our National Science Foundation Continental Dynamics group. Petr Yakovlev, Jiang Yi, and Zhang Peng provided considerable assistance in the field. Special thanks to Amanda Maslyn for assistance in apatite and zircon separation; to Stuart Thomson and Eva Enkelmann for fission track analysis; to Jim Metcalf for U, Th, and Sm measurement; and to Chris Hall for $^{40}\text{Ar}/^{39}\text{Ar}$ analyses. We thank Richard Lease, Jingen Dai, and an anonymous reviewer for their constructive reviews of this manuscript.

References

- Armijo, R., Tapponnier, P., & Han, T. L. (1989). Late Cenozoic faulting in southern Tibet. *Journal of Geophysical Research*, 94(B3), 2787–2838. <https://doi.org/10.1029/JB094iB03p02787>
- Armijo, R., Tapponnier, P., Mercier, J. L., & Tonglin, H. (1986). Quaternary extension in southern Tibet: Field observations and tectonic implications. *Journal of Geophysical Research*, 91, 13,803–13,872.
- Arnaud, N. O., Tapponnier, P., Roger, F., Brunel, M., Scharer, U., Wen, C., & Zhiqin, X. (2003). Evidence for Mesozoic shear along the western Kunlun and Altyn-Tagh fault, northern Tibet (China). *Journal of Geophysical Research*, 108(B1), 2053. <https://doi.org/10.1029/2001JB000904>
- Arnaud, N. O., Vidal, P., Tapponnier, P., Matte, P., & Deng, W. M. (1992). The high K_2O volcanism of northwestern Tibet: Geochemistry and tectonic implications. *Earth and Planetary Science Letters*, 111(2–4), 351–367. [https://doi.org/10.1016/0012-821X\(92\)90189-3](https://doi.org/10.1016/0012-821X(92)90189-3)
- Avouac, J.-P., & Tapponnier, P. (1993). Kinematic model of active deformation in central Asia. *Geophysical Research Letters*, 20(10), 895–898. <https://doi.org/10.1029/93GL00128>
- Benowitz, J. A., Layer, P. W., Armstrong, P., Perry, S. E., Haeussler, P. J., Fitzgerald, P. G., & Van Laningham, S. (2011). Spatial variations in focused exhumation along a continental-scale strike-slip fault: The Denali fault of the eastern Alaska Range. *Geosphere*, 7(2), 455–467. <https://doi.org/10.1130/GES00589.1>
- Biddle, K. T., & Christie-Blick, N. (Eds.) (1985). *Strike-slip deformation, basin formation, and sedimentation* (Vol. 37, p. 356). SEPM Society for Sedimentary Geology.
- Bilham, R., & King, G. (1989). The morphology of strike-slip faults—Examples from the San Andreas Fault, California. *Journal of Geophysical Research*, 94, 10,204–10,216.
- Blisniuk, P. M., Hacker, B. R., Glodny, J., Ratschbacher, L., Bi, S., Wu, Z., et al. (2001). Normal faulting in central Tibet since at least 13.5 Myr ago. *Nature*, 412, 628–632.
- Braun, J. (2005). Quantitative constraints on the rate of landform evolution derived from low-temperature thermochronology. *Reviews in Mineralogy and Geochemistry*, 58(1), 351–374. <https://doi.org/10.2138/rmg.2005.58.13>
- Burg, J. P., Proust, F., Tapponnier, P., & Chen, G. M. (1983). Deformation phases and tectonic evolution of the Lhasa block. *Eclogae Geologicae Helveticae*, 76, 643–683.
- Burke, K., & Sengor, C. (1986). Tectonic escape in the evolution of the continental crust: Reflection seismology. *The Continental Crust*, 14, 41–53. <https://doi.org/10.1029/GD014p0041>
- Chen, J.-L., Xu, J.-F., Wang, B.-D., & Kang, Z.-Q. (2012). Cenozoic Mg-rich potassic rocks in the Tibetan Plateau: Geochemical variations, heterogeneity of subcontinental lithospheric mantle and tectonic implications. *Journal of Asian Earth Sciences*, 53, 115–130. <https://doi.org/10.1016/j.jseas.2012.03.003>
- Chen, W., Zhang, Y., Ji, Q., Wang, S., & Zhang, J. (2002). Magmatism and deformation times of the Xidatan rock series, East Kunlun Mountains. *Science in China, Series B Chemistry*, 45(S1), 20–27. <https://doi.org/10.1007/BF02932203>
- Chinnery, M. A. (1965). The vertical displacements associated with transcurrent faulting. *Journal of Geophysical Research*, 70. <https://doi.org/10.1029/JZ070;018p04627>
- Chung, S.-L., Chu, M.-F., Zhang, Y., Xie, Y., Lo, C.-H., Lee, T.-Y., et al. (2005). Tibetan tectonic evolution inferred from spatial and temporal variations in post-collisional magmatism. *Earth-Science Reviews*, 68(3–4), 173–196. <https://doi.org/10.1016/j.earscirev.2004.05.001>
- Clark, M. K. (2012). Continental collision slowing due to viscous mantle lithosphere rather than topography. *Nature*, 483(7387), 74–77. <https://doi.org/10.1038/nature10848>
- Clark, M. K., Bush, J. W. M., & Royden, L. H. (2005). Dynamic topography produced by lower crustal flow against rheological strength heterogeneities bordering the Tibetan Plateau. *Geophysical Journal International*, 162(2), 575–590. <https://doi.org/10.1111/j.1365-246X.2005.02580.x>
- Clark, M. K., Farley, K. A., Zheng, D., Wang, Z., & Duvall, A. R. (2010). Early Cenozoic faulting of the northern Tibetan Plateau margin from apatite (U–Th)/He ages. *Earth and Planetary Science Letters*, 296(1–2), 78–88. <https://doi.org/10.1016/j.epsl.2010.04.051>

- Clark, M. K., House, M. A., Royden, L. H., Whipple, K., Burchfiel, B. C., Zhang, X., & Tang, W. (2005). Late Cenozoic uplift of southeastern Tibet. *Geology*, 33(6), 525–528. <https://doi.org/10.1130/G21265.1>
- Clark, M. K., & Royden, L. H. (2000). Topographic ooze: Building the eastern margin of Tibet by lower crustal flow. *Geology*, 28(8), 703–706.
- Crowell, J. C. (1974). Origin of late Cenozoic basins in southern California, in tectonics and sedimentation. *Society of Economic Paleontologists and Mineralogists. Special Publication*, 22, 190–204.
- Dai, J., Wang, C., Hourigan, J., & Santosh, M. (2013). Multi-stage tectono-magmatic events of the eastern Kunlun range, northern Tibet: Insights from U-Pb geochronology and (U-Th)/He thermochronology. *Tectonophysics*, 599, 97–106. <https://doi.org/10.1016/j.tecto.2013.04.005>
- Dazé, A., Lee, J. K., & Villeneuve, M. (2003). An intercalibration study of the Fish Canyon sanidine and biotite $^{40}\text{Ar}/^{39}\text{Ar}$ standards and some comments on the age of the Fish Canyon Tuff. *Chemical Geology*, 199(1–2), 111–127. [https://doi.org/10.1016/S0009-2541\(03\)00079-2](https://doi.org/10.1016/S0009-2541(03)00079-2)
- DeCelles, P. G., Kapp, P., Ding, L., & Gehrels, G. E. (2007). Late Cretaceous to middle Tertiary basin evolution in the central Tibetan Plateau: Changing environments in response to tectonic partitioning, aridification, and regional elevation gain. *Geological Society of America Bulletin*, 119(5–6), 654–680. <https://doi.org/10.1130/B26074.1>
- DeCelles, P. G., Kapp, P., Quade, J., & Gehrels, G. E. (2011). Oligocene-Miocene Kailas basin, southwestern Tibet: Record of postcollisional upper-plate extension in the Indus-Yarlung suture zone. *GSA Bulletin*, 123(7–8), 1337–1362.
- DeCelles, P. G., Quade, J., Kapp, P., Fan, M., Dettman, D. L., & Ding, L. (2007). High and dry in central Tibet during the Late Oligocene. *Earth and Planetary Science Letters*, 253(3–4), 389–401. <https://doi.org/10.1016/j.epsl.2006.11.001>
- Ding, L., Kapp, P., Yue, Y., & Lai, Q. (2007). Postcollisional calc-alkaline lavas and xenoliths from the southern Qiangtang terrane, central Tibet. *Earth and Planetary Science Letters*, 254(1–2), 28–38. <https://doi.org/10.1016/j.epsl.2006.11.019>
- Ding, L., Kapp, P., Zhong, D., & Deng, W. (2003). Cenozoic volcanism in Tibet: Evidence for a transition from oceanic to continental subduction. *Journal of Petrology*, 44, 1833–1865.
- Ding, L., Xu, Q., Yue, Y., Wang, H., Cai, F., & Li, S. (2014). The Andean-type Gangdese Mountains: Paleoelevation record from the Paleocene–Eocene Linzhou Basin. *Earth and Planetary Science Letters*, 392, 250–264. <https://doi.org/10.1016/j.epsl.2014.01.045>
- Dong, H., Hall, C. M., Peacor, D. R., & Halliday, A. N. (1995). Mechanisms of argon retention in clays revealed by laser $^{40}\text{Ar}/^{39}\text{Ar}$ dating. *Science*, 267(5196), 355–359. <https://doi.org/10.1126/science.267.5196.355>
- Dupont-Nivet, G., Lippert, P. C., van Hinsbergen, D. J., Meijers, M. J., & Kapp, P. (2010). Palaeolatitude and age of the Indo–Asia collision: Palaeomagnetic constraints. *Geophysical Journal International*, 182(3), 1189–1198. <https://doi.org/10.1111/j.1365-246X.2010.04697.x>
- Duvall, A. R., Clark, M. K., Kirby, E., Farley, K. A., Craddock, W. H., Li, C., & Yuan, D.-Y. (2013). Low-temperature thermochronometry along the Kunlun and Haiyuan Faults, NE Tibetan Plateau: Evidence for kinematic change during late-stage orogenesis. *Tectonics*, 32(5), 1190–1211. <https://doi.org/10.1002/tect.20072>
- Duvall, A. R., Clark, M. K., van der Pluijm, B. A., & Li, C. (2011). Direct dating of Eocene reverse faulting in northeastern Tibet using Ar-dating of fault clays and low-temperature thermochronometry. *Earth and Planetary Science Letters*, 304(3–4), 520–526. <https://doi.org/10.1016/j.epsl.2011.02.028>
- Ehlers, T. A., & Farley, K. A. (2003). Apatite (U-Th)/He thermochronometry: Methods and applications to problems in tectonic and surface processes. *Earth and Planetary Science Letters*, 206, 1–14.
- England, P., & Houseman, G. (1989). Extension during continental convergence, with application to the Tibetan Plateau. *Journal of Geophysical Research*, 94(B12), 17,561–17,579.
- England, P., & Searle, M. (1986). The Cretaceous-Tertiary deformation of the Lhasa block and its implications for crustal thickening in Tibet. *Tectonics*, 5(1), 1–14. <https://doi.org/10.1029/TC005i001p00001>
- Farley, K. A., & Stockli, D. F. (2002). (U-Th)/He dating of phosphates: Apatite, monazite, and xenotime. *Reviews in Mineralogy and Geochemistry*, 48(1), 559–577. <https://doi.org/10.2138/rmg.2002.48.15>
- Flowers, R. M., Ketcham, R. A., Shuster, D. L., & Farley, K. A. (2009). Apatite (U-Th)/He thermochronometry using a radiation damage accumulation and annealing model. *Geochimica et Cosmochimica Acta*, 73(8), 2347–2365. <https://doi.org/10.1016/j.gca.2009.01.015>
- Fu, B., & Awata, Y. (2007). Displacement and timing of left-lateral faulting in the Kunlun Fault zone, northern Tibet, inferred from geologic and geomorphic features. *Journal of Asian Earth Sciences*, 29(2–3), 253–265. <https://doi.org/10.1016/j.jseas.2006.03.004>
- Fu, B. H., Walker, R., & Sandiford, M. (2011). The 2008 Wenchuan earthquake and active tectonics of Asia. *Journal of Asian Earth Sciences*, 40(4), 797–804. <https://doi.org/10.1016/j.jseas.2011.01.003>
- Galbraith, R. F. (1981). On statistical models for fission track counts. *Journal of the International Association for Mathematical Geology*, 13(6), 471–478.
- Gallagher, K. (2012). Transdimensional inverse thermal history modeling for quantitative thermochronology. *Journal of Geophysical Research*, 117, B02408. <https://doi.org/10.1029/2011JB008825>
- Garzione, C. N., DeCelles, P. G., Hodkinson, D. G., Ojha, T. P., & Upreti, B. N. (2003). East-west extension and Miocene environmental change in the southern Tibetan Plateau: Thakkhola graben, central Nepal. *Geological Society of America Bulletin*, 115(1), 3–20. [https://doi.org/10.1130/0016-7606\(2003\)115<0003:EWEAME>2.0.CO;2](https://doi.org/10.1130/0016-7606(2003)115<0003:EWEAME>2.0.CO;2)
- Grathoff, G. H., & Moore, D. M. (1996). Illite polytype quantification using Wildfire© calculated X-ray diffraction patterns. *Clays and Clay Minerals*, 44(6), 835–842.
- Guo, Z., Wilson, M., Liu, J., & Mao, Q. (2006). Post-collisional, potassic and ultrapotassic magmatism of the northern Tibetan Plateau: Constraints on characteristics of the mantle source, geodynamic setting and uplift mechanisms. *Journal of Petrology*, 47(6), 1177–1220. <https://doi.org/10.1093/ptrology/egl007>
- Guo, Z., Wilson, M., Zhang, L., Zhang, M., Cheng, Z., & Liu, J. (2014). The role of subduction channel mélanges and convergent subduction systems in the petrogenesis of post-collisional K-rich mafic magmatism in NW Tibet. *Lithos*, 198–199, 184–201. <https://doi.org/10.1016/j.lithos.2014.03.020>
- Haines, S. H., & van der Pluijm, B. A. (2008). Clay quantification and Ar–Ar dating of synthetic and natural gouge: Application to the Miocene Sierra Mazatán detachment fault, Sonora, Mexico. *Journal of Structural Geology*, 30(4), 525–538. <https://doi.org/10.1016/j.jsg.2007.11.012>
- Hetzl, R., Dunkl, I., Haider, V., Strobl, M., Von Eynatten, H., Ding, L., & Frei, D. (2011). Peneplain formation in southern Tibet predates the India-Asia collision and plateau uplift. *Geology*, 39(10), 983–986. <https://doi.org/10.1130/G32069.1>
- Hough, B. G., Garzione, C. N., Wang, Z. C., Lease, R. O., Burbank, D. W., & Yuan, D. Y. (2011). Stable isotope evidence for topographic growth and basin segmentation: Implications for the evolution of the NE Tibetan Plateau. *Geological Society of America Bulletin*, 123(1–2), 168–185. <https://doi.org/10.1130/B30090.1>

- Jiang, C., Yang, Y., & Zheng, Y. (2014). Penetration of mid-crustal low velocity zone across the Kunlun Fault in the NE Tibetan Plateau revealed by ambient noise tomography. *Earth and Planetary Science Letters*, 406, 81–92. <https://doi.org/10.1016/j.epsl.2014.08.040>
- Jiang, D., Liu, J., & Ding, L. (2008). Geochemistry and petrogenesis of Cenozoic potassic volcanic rocks in the Hoh Xil area, northern Tibet Plateau. *Acta Petrologica Sinica*, 24, 279–290. CNKI:SUN:YSSXB.0.2008-02-010
- Jiang, Y.-H., Jiang, S.-Y., Ling, H.-F., & Dai, B.-Z. (2006). Low-degree melting of a metasomatized lithospheric mantle for the origin of Cenozoic Yulong monzogranite-porphyry, east Tibet: Geochemical and Sr–Nd–Pb–Hf isotopic constraints. *Earth and Planetary Science Letters*, 241(3–4), 617–633. <https://doi.org/10.1016/j.epsl.2005.11.023>
- Jolivet, M., Brunel, M., Seward, D., Xu, Z., Yang, J., Malavieille, J., et al. (2003). Neogene extension and volcanism in the Kunlun Fault zone, northern Tibet: New constraints on the age of the Kunlun Fault. *Tectonics*, 22(5), 1052. <https://doi.org/10.1029/2002TC001428>
- Kapp, P., DeCelles, P. G., Gehrels, G. E., Heizler, M., & Ding, L. (2007). Geological records of the Lhasa-Qiangtang and Indo-Asian collisions in the Nima area of central Tibet. *Geological Society of America Bulletin*, 119(7–8), 917–933. <https://doi.org/10.1130/B26033.1>
- Kapp, P., DeCelles, P. G., Leier, A. L., Fabijanic, J. M., He, S., Pullen, A., & Gehrels, G. E. (2007). The Gangdese retroarc thrust belt revealed. *GSA Today*, 17(7), 4–9. <https://doi.org/10.1130/GSAT01707A.1>
- Kapp, P., Murphy, M. A., Yin, A., Harrison, T. M., Ding, L., & Guo, J. (2003). Mesozoic and Cenozoic tectonic evolution of the Shiquanhe area of western Tibet. *Tectonics*, 22(4). <https://doi.org/10.1029/2001tc001332>
- Kapp, P., Yin, A., Harrison, T. M., & Ding, L. (2005). Cretaceous–Tertiary shortening, basin development, and volcanism in central Tibet. *Geological Society of America Bulletin*, 117(7), 865–878. <https://doi.org/10.1130/B25595.1>
- Karner, D. B., & Renne, P. R. (1998). ⁴⁰Ar/³⁹Ar geochronology of Roman volcanic province tephra in the Tiber River valley: Age calibration of middle Pleistocene sea-level changes. *Geological Society of America Bulletin*, 110, 740–747. [https://doi.org/10.1130/0016-7606\(1998\)110<0740](https://doi.org/10.1130/0016-7606(1998)110<0740)
- Karplus, M. S., Zhao, W., Klemperer, S. L., Wu, Z., Mechie, J., Shi, D., et al. (2011). Injection of Tibetan crust beneath the south Qaidam Basin: Evidence from INDEPTH IV wide-angle seismic data. *Journal of Geophysical Research*, 116, B07301. <https://doi.org/10.1029/2010JB007911>
- Kidd, W. S., & Molnar, P. (1988). Quaternary and active faulting observed on the 1985 Academia Sinica-Royal Society Geotraverse of Tibet. *Philosophical transactions of the Royal Society of London. Series A, Mathematical and Physical Sciences*, 327, 337–363.
- Kidd, W. S., Pan, Y., Chang, C., Coward, M. P., Dewey, J. F., Gansser, A., et al. (1988). Geological mapping of the 1985 Chinese-British Tibetan (Xizang-Qinghai) Plateau Geotraverse route. *Philosophical transactions of the Royal Society of London. Series A, Mathematical and Physical Sciences*, 327, 287–305.
- Kirby, E., Harkins, N., Wang, E., Shi, X., Fan, C., & Burbank, D. (2007). Slip rate gradients along the eastern Kunlun fault. *Tectonics*, 26, TC2010. <https://doi.org/10.1029/2006TC002033>
- Klemperer, S. L. (2006). Crustal flow in Tibet: Geophysical evidence for the physical state of Tibetan lithosphere, and inferred patterns of active flow. *Geological Society of London, Special Publication*, 268(1), 39–70. <https://doi.org/10.1144/GSL.SP.2006.268.01.03>
- Lai, S.-C., Liu, C.-Y., & Yi, H.-S. (2003). Geochemistry and petrogenesis of Cenozoic andesite-dacite associations from the Hoh Xil region, Tibetan Plateau. *International Geology Review*, 45(11), 998–1019. <https://doi.org/10.2747/0020-6814.45.11.998>
- Lease, R. O., Burbank, D. W., Clark, M. K., Farley, K. A., Zheng, D., & Zhang, H. (2011). Middle Miocene reorganization of deformation along the northeastern Tibetan Plateau. *Geology*, 39(4), 359–362. <https://doi.org/10.1130/G31356.1>
- Lease, R. O., Burbank, D. W., Hough, B., Wang, Z., & Yuan, D. (2012). Pulsed Miocene range growth in northeastern Tibet: Insights from Xunhua Basin magnetostratigraphy and provenance. *Geological Society of America Bulletin*, 124(5–6), 657–677. <https://doi.org/10.1130/B30524.1>
- Lee, H.-Y., Chung, S.-L., Wang, J.-R., Wen, D.-J., Lo, C.-H., Yang, T. F., et al. (2003). Miocene Jiali faulting and its implications for Tibetan tectonic evolution. *Earth and Planetary Science Letters*, 205(3–4), 185–194. [https://doi.org/10.1016/S0012-821X\(02\)01040-3](https://doi.org/10.1016/S0012-821X(02)01040-3)
- Lee, J., Hager, C., Wallis, S. R., Stockli, D. F., Whitehouse, M. J., Aoya, M., & Wang, Y. (2011). Middle to late Miocene extremely rapid exhumation and thermal reequilibration in the Kung Co rift, southern Tibet. *Tectonics*, 30, TC2007. <https://doi.org/10.1029/2010TC002745>
- Li, G. W., Sandiford, M., Fang, A. M., Kohn, B., Sandiford, D., Fu, B. H., et al. (2019). Multi-stage exhumation history of the West Kunlun orogen and the amalgamation of the Tibetan Plateau. *Earth and Planetary Science Letters*, 528. <https://doi.org/10.1016/j.epsl.2019.115833>
- Li, H. B., Van der Woerd, J., Tapponnier, P., Klinger, Y., Qi, X. X., Yang, J. S., & Zhu, Y. T. (2005). Slip rate on the Kunlun fault at Hongshui Gou, and recurrence time of great events comparable to the 14/11/2001, Mw ~ 7.9 Kokoxili earthquake. *Earth and Planetary Science Letters*, 237(1), 285–299.
- Lin, J., Dai, J. G., Zhuang, G., Jia, G., Zhang, L., Ning, Z., et al. (2020). Late Eocene-Oligocene high relief paleotopography in the north central Tibetan Plateau: Insights from detrital zircon U-Pb geochronology and leaf wax hydrogen isotope studies. *Tectonics*, 39, e2019TC005815. <https://doi.org/10.1029/2019TC005815>
- Liu, Y., Genser, J., Neubauer, F., Jin, W., Ge, X., Handler, R., & Takasu, A. (2005). ⁴⁰Ar/³⁹Ar mineral ages from basement rocks in the eastern Kunlun Mountains, NW China, and their tectonic implications. *Tectonophysics*, 398(3–4), 199–224. <https://doi.org/10.1016/j.tecto.2005.02.007>
- Malusà, M. G., & Fitzgerald, P. G. (2019). Application of thermochronology to geologic problems: Bedrock and detrital approaches. In *Fission-track thermochronology and its application to geology* (pp. 191–209). Cham, Switzerland: Springer.
- McCallister, A. T., Taylor, M. H., Murphy, M. A., Styron, R. H., & Stockli, D. F. (2013). Thermochronologic constraints on the late Cenozoic exhumation history of the Gurla Mandhata metamorphic core complex, southwestern Tibet. *Tectonics*, 33, 27–52. <https://doi.org/10.1002/2013TC003302>
- McKenna, L. W., & Walker, J. D. (1990). Geochemistry of crustally derived leucocratic igneous rocks from the Ulugh Muztagh area, northern Tibet and their implications for the formation of the Tibetan Plateau. *Journal of Geophysical Research*, 95(B13), 21,483–21,502. <https://doi.org/10.1029/jb095ib13p21483>
- McRivette, M. W., Yin, A., Chen, X., & Gehrels, G. E. (2019). Cenozoic basin evolution of the central Tibetan Plateau as constrained by U-Pb detrital zircon geochronology, sandstone petrology, and fission-track thermochronology. *Tectonophysics*, 751, 150–179. <https://doi.org/10.1016/j.tecto.2018.12.015>
- Miller, C., Schuster, R., Klotzli, U., Frank, W., & Purtscheller, F. (1999). Post-collisional potassic and ultrapotassic magmatism in SW Tibet: Geochemical and Sr–Nd–Pb–O isotopic constraints for mantle source characteristics and petrogenesis. *Journal of Petrology*, 40(9), 1399–1424. <https://doi.org/10.1093/ptro/40.9.1399>

- Mock, C., Arnaud, N. O., & Cantagrel, J. (1999). An early unroofing in northeastern Tibet? Constraints from $^{40}\text{Ar}/^{39}\text{Ar}$ thermochronology on granitoids from the eastern Kunlun range. *Earth and Planetary Science Letters*, 171(1), 107–122. [https://doi.org/10.1016/S0012-821X\(99\)00133-8](https://doi.org/10.1016/S0012-821X(99)00133-8)
- Molnar, P., England, P., & Martinod, J. (1993). Mantle dynamics, uplift of the Tibetan Plateau, and the Indian Monsoon. *Reviews in Geophysics*, 31(4), 357–396.
- Molnar, P., & Stock, J. M. (2009). Slowing of India's convergence with Eurasia since 20 Ma and its implications for Tibetan mantle dynamics. *Tectonics*, 28, TC3001. <https://doi.org/10.1029/2008TC002271>
- Molnar, P., & Tapponnier, P. (1978). Active faulting in Tibet. *Journal of Geophysical Research*, 83(B11), 5361–5375. <https://doi.org/10.1029/JB083iB11p05361>
- Murphy, M. A., Manning, C. E., Ryerson, F. J., & Lin, D. (2002). Structural evolution of the Gurla Mandhata detachment system, southwest Tibet: Implications for the eastward extent of the Karakoram fault system. *GSA Bulletin*, 114, 428–447.
- Murphy, M. A., Yin, A., Harrison, T. M., Dürr, S. B., Chen, Z., Ryerson, F. J., et al. (1997). Did the Indo-Asian collision alone create the Tibetan Plateau? *Geology*, 25(8), 719–722. [https://doi.org/10.1130/0091-7613\(1997\)025<0719:DTIACA>2.3.CO;2](https://doi.org/10.1130/0091-7613(1997)025<0719:DTIACA>2.3.CO;2)
- Murphy, M. A., Yin, A., Kapp, P., Harrison, T. M., Ding, L., & Jinghui, G. (2000). Southward propagation of the Karakoram fault system, southwest Tibet: Timing and magnitude of slip. *Geology*, 28, 451–454.
- Najman, Y., Appel, E., Boudagher-Fadel, M., Bown, P., Carter, A., Garzanti, E., et al. (2010). Timing of India-Asia collision: Geological, biostratigraphic, and palaeomagnetic constraints. *Journal of Geophysical Research*, 115, B12416. <https://doi.org/10.1029/2010JB007673>
- Niemi, N. A., Buscher, J. T., Spotila, J. A., House, M. A., & Kelley, S. A. (2013). Insights from low-temperature thermochronometry into transpressional deformation and crustal exhumation along the San Andreas fault in the western Transverse Ranges, California. *Tectonics*, 32, 1602–1622. <https://doi.org/10.1002/2013TC003377>
- Niemi, N. A., & Clark, M. K. (2017). Long-term exhumation rates exceed paleoseismic slip rates in the central Santa Monica Mountains, Los Angeles County, California. *Geology*, 46(1), 63–66. <https://doi.org/10.1130/G39388.1>
- Nomade, S., Renne, P. R., Mo, X., Zhao, Z., & Zhou, S. (2004). Miocene volcanism in the Lhasa block, Tibet: Spatial trends and geodynamic implications. *Earth and Planetary Science Letters*, 221(1–4), 227–243. [https://doi.org/10.1016/S0012-821X\(04\)00072-X](https://doi.org/10.1016/S0012-821X(04)00072-X)
- Ouimet, W., Whipple, K., Royden, L., Reiners, P., Hodges, K., & Pringle, M. (2010). Regional incision of the eastern margin of the Tibetan Plateau. *Lithosphere*, 2, 50–63. <https://doi.org/10.1130/L57.1>
- Owens, T. J., & Zandt, G. (1997). Implications of crustal property variations for models of Tibetan Plateau evolution. *Nature*, 387(6628), 37–43. <https://doi.org/10.1038/387037a0>
- Phillips, R. J., Parrish, R. R., & Searle, M. P. (2004). Age constraints on ductile deformation and long-term slip rates along the Karakoram fault zone. *Ladakh*, 226(3–4), 305–319. <https://doi.org/10.1016/j.epsl.2004.07.037>
- Platt, J. P., & England, P. C. (1994). Convective removal of lithosphere beneath mountain belts; thermal and mechanical consequences. *American Journal of Science*, 294(3), 307–336. <https://doi.org/10.2475/ajs.294.3.307>
- Polissar, P. J., Freeman, K. H., Rowley, D. B., McInerney, F. A., & Currie, B. S. (2009). Paleoaltimetry of the Tibetan Plateau from D/H ratios of lipid biomarkers. *Earth and Planetary Science Letters*, 287(1–2), 64–76. <https://doi.org/10.1016/j.epsl.2009.07.037>
- Qinghai Bureau of Geology and Mineral Resources (QBGM) (1980). *Geologic map of the Dongwenquan region* (scale 1:200,000).
- Qinghai Bureau of Geology and Mineral Resources (QBGM) (1981). *Geologic map of the Aikendele site region* (scale 1:200,000).
- Ratschbacher, L., Krumrei, L., Lumenwitz, M., Staiger, M., Gloaguen, R., Miller, B. V., et al. (2011). Rifting and strike-slip shear in central Tibet and the geometry, age and kinematics of upper crustal extension in Tibet. *Geological Society - Special Publications*, 353(1), 127–163. <https://doi.org/10.1144/SP353.8>
- Reiners, P. W., & Farley, K. A. (2001). Influence of crystal size on apatite (U-Th)/He thermochronology and example from the Bighorn Mountains, Wyoming. *Earth and Planetary Science Letters*, 188, 413–420.
- Renne, P. R., Swisher, C. C., Deino, A. L., Karner, D. B., Owens, T. L., & Depaolo, D. J. (1998). Intercalibration of standards, absolute ages and uncertainties in $^{40}\text{Ar}/^{39}\text{Ar}$ dating. *Chemical Geology*, 145(1–2), 117–152. [https://doi.org/10.1016/S0009-2541\(97\)00159-9](https://doi.org/10.1016/S0009-2541(97)00159-9)
- Rey, P., Vanderhaeghe, O., & Teyssier, C. (2001). Gravitational collapse of the continental crust: Definition, regimes and modes. *Tectonophysics*, 342(3–4), 435–449. [https://doi.org/10.1016/S0040-1951\(01\)00174-3](https://doi.org/10.1016/S0040-1951(01)00174-3)
- Ritts, B. D., Yue, Y., Graham, S. a., Sobel, E. R., Abbink, O. a., & Stockli, D. (2008). From sea level to high elevation in 15 million years: Uplift history of the northern Tibetan Plateau margin in the Altun Shan. *American Journal of Science*, 308(5), 657–678. <https://doi.org/10.2475/05.2008.01>
- Rohrmann, A., Kapp, P., Carrapa, B., Reiners, P. W., Guynn, J., Ding, L., & Heizler, M. (2012). Thermochronologic evidence for plateau formation in central Tibet by 45 Ma. *Geology*, 40(2), 187–190. <https://doi.org/10.1130/G32530.1>
- Rowley, D. B. (1996). Age of initiation of collision between India and Asia: A review of stratigraphic data. *Earth and Planetary Science Letters*, 145, 1–13.
- Rowley, D. B., & Currie, B. S. (2006). Palaeo-altimetry of the late Eocene to Miocene Lunpola basin, central Tibet. *Nature*, 439(7077), 677–681. <https://doi.org/10.1038/nature04506>
- Royden, L., Burchfiel, B., King, R., Wang, E., Chen, Z., Shen, F., & Liu, Y. (1997). Surface deformation and lower crustal flow in eastern Tibet. *Science*, 276(5313), 788–790. <https://doi.org/10.1126/science.276.5313.788>
- Shi, W. B., Wang, F., Wu, L., Yang, L. K., Zhang, W. B., & Wang, Y. Z. (2018). A prolonged Cenozoic erosional period in East Kunlun (Western China): Constraints of detrital apatite (U-Th)/He ages on the onset of mountain building along the northern margin of the Tibetan Plateau. *Journal of Asian Earth Sciences*, 151, 54–61.
- Spotila, J., Farley, K. A., & Sich, K. (1998). Uplift and erosion of the San Bernardino Mountains associated with transpression along the San Andreas fault, California, as constrained by radiogenic helium thermochronometry. *Tectonics*, 17, 360–378.
- Spotila, J. A., Farley, K. A., Yule, J. D., & Reiners, P. W. (2001). Near-field transpressive deformation along the San Andreas fault zone in southern California, based on exhumation constrained by (U-Th)/He dating. *Journal of Geophysical Research*, 106, 30909. <https://doi.org/10.1029/2001JB000348>
- Spotila, J. A., Niemi, N., Brady, R., House, M., Buscher, J., & Oskin, M. (2007). Long-term continental deformation associated with transpressive plate motion: The San Andreas fault. *Geology*, 35, 967. <https://doi.org/10.1130/G23816A.1>
- Staisch, L. M., Niemi, N. A., Chang, H., Clark, M. K., Rowley, D. B., & Currie, B. S. (2014). A Cretaceous-Eocene depositional age for the Fenghuoshan group, Hoh Xil Basin: Implications for the tectonic evolution of the northern Tibet Plateau. *Tectonics*, 33, 281–301. <https://doi.org/10.1002/2013TC003367>
- Staisch, L. M., Niemi, N. A., Clark, M. K., & Hong, C. (2016). Eocene-late Oligocene history of crustal shortening within the Hoh Xil Basin and implications for the uplift history of the northern Tibetan Plateau. *Tectonics*, 35, 862–895. <https://doi.org/10.1002/2015TC003972>

- Styron, R., Taylor, M., & Okoronkwo, K. (2010). Database of active structures from the Indo-Asian collision. *Eos, Transactions American Geophysical Union*, 91(20), 181–182. <https://doi.org/10.1029/2010EO200001>
- Styron, R. H., Taylor, M. H., Sundell, K. E., Stockli, D. F., Oalmann, J. A. G., Möller, A., et al. (2013). Miocene initiation and acceleration of extension in the South Lunggar rift, western Tibet: Evolution of an active detachment system from structural mapping and (U-Th)/He thermochronology. *Tectonics*, 32, 880–907. <https://doi.org/10.1002/tect.20053>
- Sun, B., Wang, Y.-F., Li, C.-S., Yang, J., Li, J.-F., Li, Y.-L., et al. (2015). Early Miocene elevation in northern Tibet estimated by palaeobotanical evidence. *Scientific Reports*, 5(1). <https://doi.org/10.1038/srep10379>
- Sundell, K. E., Taylor, M. H., Styron, R. H., Stockli, D. F., Kapp, P., Hager, C., et al. (2013). Evidence for constriction and Pliocene acceleration of east-west extension in the North Lunggar rift region of west central Tibet. *Tectonics*, 32, 1454–1479. <https://doi.org/10.1002/tect.20086>
- Taylor, M., & Peltzer, G. (2006). Current slip rates on conjugate strike-slip faults in central Tibet using synthetic aperture radar interferometry. *Journal of Geophysical Research*, 111, B12402. <https://doi.org/10.1029/2005JB004014>
- Taylor, M., Yin, A., Ryerson, F. J., Kapp, P., & Ding, L. (2003). Conjugate strike-slip faulting along the Bangong-Nujiang suture zone accommodates coeval east-west extension and north-south shortening in the interior of the Tibetan Plateau. *Tectonics*, 22(4), 1044. <https://doi.org/10.1029/2002TC001361>
- Turner, S., Arnaud, N., Liu, J., Rogers, N., Hawkesworth, C., Harris, N., et al. (1996). Post-collision, shoshonitic volcanism on the Tibetan Plateau: Implications for convective thinning of the lithosphere and the source of ocean island basalts. *Journal of Petrology*, 37(1), 45–71. <https://doi.org/10.1093/petrology/37.1.45>
- Turner, S., Hawkesworth, C., Liu, J., Rogers, N., Kelley, S. P., & van Calsteren, P. (1993). Timing of Tibetan uplift constrained by analysis of volcanic rocks. *Nature*, 364(6432), 50–54. <https://doi.org/10.1038/364050a0>
- van der Pluijm, B. A., Hall, C. M., Vrolijk, P. J., Pevear, D. R., & Covey, M. C. (2001). The dating of shallow faults in the Earth's crust. *Nature*, 412, 172–175. <https://doi.org/10.1038/35084053>
- van der Woerd, J., Ryerson, F. J., Tapponnier, P., Gaudemer, Y., Finkel, R. C., Meriaux, A.-S., et al. (1998). Holocene left-slip rate determined by cosmogenic surface dating on the Xidatan segment of the Kunlun fault (Qinghai, China). *Geology*, 26(8), 695–698. [https://doi.org/10.1130/0091-7613\(1998\)026<0695](https://doi.org/10.1130/0091-7613(1998)026<0695)
- van der Woerd, J., Ryerson, F. J., Tapponnier, P., Meriaux, A. S., Gaudemer, Y., Meyer, B., et al. (2000). Uniform slip-rate along the Kunlun Fault: Implications for seismic behaviour and large-scale tectonics. *Geophysical Research Letters*, 27(16), 2353–2356.
- van der Woerd, J., Tapponnier, P., Ryerson, F. J., Meriaux, A., Meyer, B., Gaudemer, Y., et al. (2002). Uniform postglacial slip-rate along the central 600 km of the Kunlun Fault (Tibet), from ²⁶Al, ¹⁰Be, ¹⁴C dating of riser offsets, and climatic origin of the regional morphology. *Geophysical Journal International*, 148(3), 356–388. <https://doi.org/10.1046/j.1365-246x.2002.01556.x>
- Verdel, C., van der Pluijm, B. A., & Niemi, N. A. (2012). Variation of illite/muscovite ⁴⁰Ar/³⁹Ar age spectra during progressive low-grade metamorphism: An example from the US Cordillera. *Contributions to Mineralogy and Petrology*, 164, 521–536. <https://doi.org/10.1007/s00410-012-0751-7>
- Wang, F., Lo, C.-H., Li, Q., Yeh, M.-W., Wan, J., Zheng, D., & Wang, E. (2004). Onset timing of significant unroofing around Qaidam basin, northern Tibet, China: Constraints from ⁴⁰Ar/³⁹Ar and FT thermochronology on granitoids. *Journal of Asian Earth Sciences*, 24, 59–69. <https://doi.org/10.1016/j.jseae.2003.07.004>
- Wang, F., Shi, W., Zhang, W., Wu, L., Yang, L., Wang, Y., & Zhu, R. (2017). Differential growth of the northern Tibetan margin: Evidence for oblique stepwise rise of the Tibetan Plateau. *Scientific Reports*, 7(1), 1–9.
- Wang, Q., Chung, S.-L., Li, X.-H., Wyman, D., Li, Z.-X., Sun, W.-D., et al. (2012). Crustal melting and flow beneath northern Tibet: Evidence from Mid-Miocene to quaternary strongly peraluminous rhyolites in the southern Kunlun Range. *Journal of Petrology*, 53(12), 2523–2566. <https://doi.org/10.1093/petrology/egs058>
- Wang, Q., McDermott, F., Xu, J., Bellon, H., & Zhu, Y. (2005). Cenozoic K-rich adakitic volcanic rocks in the Hohxil area, northern Tibet: Lower-crustal melting in an intracontinental setting. *Geology*, 33(6), 465–468. <https://doi.org/10.1130/G21522.1>
- Wang, S., Fang, X., Zheng, D., & Wang, E. (2009). Initiation of slip along the Xianshuihe fault zone, eastern Tibet, constrained by K/Ar and fission-track ages. *International Geology Review*, 51(12), 1121–1131. <https://doi.org/10.1080/00206810902945132>
- Wang, Z., Zhang, P., Garzone, C. N., Lease, R. O., Zhang, G., Zheng, D., et al. (2012). Magnetostratigraphy and depositional history of the Miocene Wushan Basin on the NE Tibetan Plateau, China: Implications for middle Miocene tectonics of the West Qinling fault zone. *Journal of Asian Earth Sciences*, 44, 189–202. <https://doi.org/10.1016/j.jseae.2011.06.009>
- Wilcox, R. E., Harding, T. T., & Seely, D. R. (1973). Basic wrench tectonics. *AAPG Bulletin*, 57, 74–96.
- Williams, H., Turner, S., Kelley, S., & Harris, N. (2001). Age and composition of dikes in Southern Tibet: New constraints on the timing of east-west extension and its relationship to postcollisional volcanism. *Geology*, 29(4), 339. [https://doi.org/10.1130/0091-7613\(2001\)029<0339:aacodi>2.0.co;2](https://doi.org/10.1130/0091-7613(2001)029<0339:aacodi>2.0.co;2)
- Williams, H. M., Turner, S. P., Pearce, J. A., Kelley, S. P., & Harris, N. B. W. (2004). Nature of the source regions for post-collisional, potassic magmatism in southern and northern Tibet from geochemical variations and inverse trace element modelling. *Journal of Petrology*, 45(3), 555–607. <https://doi.org/10.1093/petrology/egg094>
- Wu, C., Zuza, A. V., Chen, X., Lin, D., Levy, D. A., Liu, C., et al. (2019). Tectonics of the eastern Kunlun range: Cenozoic reactivation of a Paleozoic-early Mesozoic Orogen. *Tectonics*, 38, 1609–1650. <https://doi.org/10.1029/2018TC005370>
- Wu, C., Zuza, A. V., Zhuo, Z., Yin, A., McRivette, M. W., Chen, X., et al. (2019). Mesozoic-Cenozoic evolution of the eastern Kunlun range, central Tibet, and implications for basin evolution during the Indo-Asian collision. *Lithosphere*, 11(4), 524–550. <https://doi.org/10.1130/L1065.1>
- Wu, F., Zhang, X. J., Zhang, Y. Q., & Zhang, Y. L. (2010). Zircon: U-Pb ages for rhyolitic tuffs of the Naocangjianguo formation in the east Kunlun orogenic belt and their implication. *Journal of Geomechanics*, 16(1), 44–50.
- Wu, Y., Cui, Z., Liu, G., Ge, D., Yin, J., Xi, Q., & Pang, Q. (2001). Quaternary geomorphological evolution of the Kunlun Pass area and uplift of the Qinghai-Xizang, Tibet Plateau. *Geomorphology*, 36, 203–216.
- Wu, Z., Barosh, P. J., Wu, Z., Hu, D., Zhao, X., & Ye, P. (2008). Vast early Miocene lakes of the central Tibetan Plateau. *Geological Society of America Bulletin*, 120(9–10), 1326–1337. <https://doi.org/10.1130/B26043.1>
- Wu, Z., Ye, P., Patrick, B. J., Hu, D., Zhao, W., & Wu, Z. (2009). Late Oligocene-Early Miocene thrusting in southern East Kunlun Mountains, northern Tibetan Plateau. *Journal of Earth Science*, 20(2), 381–390. <https://doi.org/10.1007/s12583-009-0031-2>
- Wu, Z. H., Ye, P. S., Zhao, W. J., Patrick, J. B., & Hu, D. (2007). Late Cenozoic overthrust system in the southern east Kunlun Mountains, China. *Geological Bulletin of China*, 26(4), 448–456. (in Chinese with English Abstract)
- Xia, L., Li, X., Ma, Z., Xu, X., & Xia, Z. (2011). Cenozoic volcanism and tectonic evolution of the Tibetan Plateau. *Gondwana Research*, 19(4), 850–866. <https://doi.org/10.1016/j.gr.2010.09.005>

- Xu, Q., Ding, L., Zhang, L., Cai, F., Lai, Q., Yang, D., & Liu-Zeng, J. (2013). Paleogene high elevations in the Qiangtang Terrane, central Tibetan Plateau. *Earth and Planetary Science Letters*, 362, 31–42. <https://doi.org/10.1016/j.epsl.2012.11.058>
- Yakovlev, P. V., Saal, A., Clark, M. K., Hong, C., Niemi, N. A., & Mallick, S. (2019). The geochemistry of Tibetan lavas: Spatial and temporal relationships, tectonic links and geodynamic implications. *Earth and Planetary Science Letters*, 520, 115–126. <https://doi.org/10.1016/j.epsl.2019.04.032>
- Yang, D., & Ding, L. (2013). Geochronology and geochemistry of the high magnesium and high potassium ultrabasic leucite basanite in northern Tibetan Plateau. *Chinese Journal of Geophysics*, 48, 449–467.
- Yin, A., Dang, Y., Zhang, M., McRivette, M. W., Burgess, W. P., & Chen, X. (2007). Cenozoic tectonic evolution of Qaidam basin and its surrounding regions (Part 2): Wedge tectonics in southern Qaidam basin and the Eastern Kunlun range. *Geological Society of America Special Papers*, 433, 369–390. [https://doi.org/10.1130/2007.2433\(18\)](https://doi.org/10.1130/2007.2433(18))
- Yin, A., Dang, Y.-Q., Wang, L.-C., Jiang, W.-M., Zhou, S.-P., Chen, X.-H., et al. (2008). Cenozoic tectonic evolution of Qaidam basin and its surrounding regions (Part 1): The southern Qilian Shan-Nan Shan thrust belt and northern Qaidam basin. *Geological Society of America Bulletin*, 120(7–8), 813–846. <https://doi.org/10.1130/B26180.1>
- Yin, A., Rumelhart, P. E., Butler, R., Cowgill, E., Harrison, T. M., Foster, D. A., et al. (2002). Tectonic history of the Altyn Tagh fault system in northern Tibet inferred from Cenozoic sedimentation. *Geological Society of America Bulletin*, 114(10), 1257–1295. [https://doi.org/10.1130/0016-7606\(2002\)114<1257:THOTAT>2.0.CO;2](https://doi.org/10.1130/0016-7606(2002)114<1257:THOTAT>2.0.CO;2)
- Yue, Y., Ritts, B. D., & Graham, S. A. (2001). Initiation and long-term slip history of the Altyn Tagh fault. *International Geology Review*, 43(12), 1087–1093. <https://doi.org/10.1080/00206810109465062>
- Yue, Y., Ritts, B. D., Graham, S. A., Wooden, J. L., Gehrels, G. E., & Zhang, Z. (2004). Slowing extrusion tectonics: Lowered estimate of post-early Miocene slip rate for the Altyn Tagh fault. *Earth and Planetary Science Letters*, 217(1–2), 111–122. [https://doi.org/10.1016/S0012-821X\(03\)00544-2](https://doi.org/10.1016/S0012-821X(03)00544-2)
- Zhuang, G., Johnstone, S. A., Hourigan, J., Ritts, B., Robinson, A., & Sobel, E. R. (2018). Understanding the geologic evolution of northern Tibetan Plateau with multiple thermochronometers. *Gondwana Research*, 58, 195–210. <https://doi.org/10.1016/j.gr.2018.02.014>